

1 **A comprehensive study of hygroscopic properties of calcium- and magnesium-**
2 **containing salts: implication for hygroscopicity of mineral dust and sea salt aerosols**

3
4 **Liya Guo,^{1,5,a} Wenjun Gu,^{1,5,a} Chao Peng,^{2,5} Weigang Wang,² Yong Jie Li,³ Taomou Zong,⁴**
5 **Yujing Tang,¹ Zhijun Wu,⁴ Qin hao Lin,¹ Maofa Ge,^{2,5,6} Guohua Zhang,¹ Min Hu,⁴ Xinhui**
6 **Bi,¹ Xinming Wang,^{1,5,6} Mingjin Tang^{1,5,*}**

7
8 1 State Key Laboratory of Organic Geochemistry and Guangdong Key Laboratory of
9 Environmental Protection and Resources Utilization, Guangzhou Institute of Geochemistry,
10 Chinese Academy of Sciences, Guangzhou 510640, China

11 2 State Key Laboratory for Structural Chemistry of Unstable and Stable Species, Institute of
12 Chemistry, Chinese Academy of Sciences, Beijing, China

13 3 Department of Civil and Environmental Engineering, Faculty of Science and Technology,
14 University of Macau, Avenida da Universidade, Taipa, Macau, China

15 4 State Key Joint Laboratory of Environmental Simulation and Pollution Control, College of
16 Environmental Sciences and Engineering, Peking University, Beijing 100871, China

17 5 University of Chinese Academy of Sciences, Beijing 100049, China

18 6 Center for Excellence in Regional Atmospheric Environment, Institute of Urban Environment,
19 Chinese Academy of Sciences, Xiamen 361021, China

20
21 ^a These two authors contributed equivalently to this work.

22 * Correspondence: Mingjin Tang (mingjintang@gig.ac.cn)

23 **Abstract**

24 Calcium- and magnesium-containing salts are important components for mineral dust and
25 sea salt aerosols, but their physicochemical properties are not well understood yet. In this study,
26 the hygroscopic properties of eight Ca- and Mg-containing salts, including $\text{Ca}(\text{NO}_3)_2 \cdot 4\text{H}_2\text{O}$,
27 $\text{Mg}(\text{NO}_3)_2 \cdot 6\text{H}_2\text{O}$, $\text{MgCl}_2 \cdot 6\text{H}_2\text{O}$, $\text{CaCl}_2 \cdot 6\text{H}_2\text{O}$, $\text{Ca}(\text{HCOO})_2$, $\text{Mg}(\text{HCOO})_2 \cdot 2\text{H}_2\text{O}$,
28 $\text{Ca}(\text{CH}_3\text{COO})_2 \cdot \text{H}_2\text{O}$ and $\text{Mg}(\text{CH}_3\text{COO})_2 \cdot 4\text{H}_2\text{O}$, were investigated using two complementary
29 techniques. A vapor sorption analyzer was used to measure the change of sample mass with relative
30 humidity (RH) under isotherm conditions, and the deliquescence relative humidities (DRH) for
31 temperature in the range of 5-30 °C as well as water-to-solute ratios as a function of RH at 5 and
32 25 °C were reported for these eight compounds. DRH values showed large variation for these
33 compounds; for example, at 25 °C DRH were measured to be ~28.5% for $\text{CaCl}_2 \cdot 6\text{H}_2\text{O}$ and >95%
34 for $\text{Ca}(\text{HCOO})_2$ and $\text{Mg}(\text{HCOO})_2 \cdot 2\text{H}_2\text{O}$. We further found that the dependence of DRH on
35 temperature can be approximated by the Clausius-Clapeyron equation. In addition, a humidity-
36 tandem differential mobility analyzer was used to measure the change in mobility diameter with
37 RH (up to 90%) at room temperature, in order to determine the hygroscopic growth factors of
38 aerosol particles generated by atomizing water solutions of these eight compounds. All the aerosol
39 particles studied in this work, very likely to be amorphous under dry conditions, started to grow at
40 very low RH (as low as 10%) and showed continuous growth with RH. The hygroscopic growth
41 factors at 90% RH were found to range from 1.26 ± 0.04 for $\text{Ca}(\text{HCOO})_2$ to 1.79 ± 0.03 for $\text{Ca}(\text{NO}_3)_2$,
42 and the single hygroscopicity parameter ranged from 0.09-0.13 for $\text{Ca}(\text{CH}_3\text{COO})_2$ to 0.49-0.56 for
43 $\text{Ca}(\text{NO}_3)_2$. Overall, our work provides a comprehensive investigation of the hygroscopic properties
44 of these Ca- and Mg-containing salts, largely improving our knowledge in the physicochemical
45 properties of mineral dust and sea salt aerosols.

46 **1 Introduction**

47 Mineral dust, mainly emitted from arid and semi-arid regions with an annual flux of
48 ~2000 Tg, is one of the most abundant types of aerosols in the troposphere (Textor et al.,
49 2006;Ginoux et al., 2012). Mineral dust aerosol affects the climate system directly by scattering
50 and absorbing solar and terrestrial radiation (Formenti et al., 2011;Ridley et al., 2016;Chen et al.,
51 2017) and indirectly by serving as cloud condensation nuclei (CCN) and ice nucleating particles
52 (INPs) (Hoose and Moehler, 2012;Creamean et al., 2013;Cziczo et al., 2013;Tang et al., 2016a).
53 In addition, deposition of mineral dust particles is an important source of several nutrient elements
54 (Fe and P, for example) for many ecosystems around the globe, thus having significant impacts on
55 biogeochemical cycles in these regions (Jickells et al., 2005;Mahowald et al., 2009;Mahowald et
56 al., 2011;Zhang et al., 2015).

57 Mineral dust aerosol has an average lifetime of 2-7 days in the atmosphere and can thus be
58 transported over thousands of kilometers (Uno et al., 2009;Textor et al., 2006). During transport
59 mineral dust particles may undergo heterogeneous reactions with trace gases, impacting the
60 abundance of a number of important reactive trace gases both directly and indirectly (Usher et al.,
61 2003;Tang et al., 2017;Crowley et al., 2010;Romanias et al., 2012). These reactions can also lead
62 to change in chemical composition of mineral dust particles (Usher et al., 2003;Li et al., 2010;Tang
63 et al., 2012;Li and Shao, 2009;Romanias et al., 2016) and thereby modification of their
64 physicochemical and optical properties (Krueger et al., 2003;Liu et al., 2008b;Tang et al.,
65 2016a;Pan et al., 2017;Sullivan et al., 2009;Vlasenko et al., 2006). Mineral dust particles contain
66 substantial amounts of carbonates, including CaCO_3 (calcite) and $\text{CaMg}(\text{CO}_3)_2$ (dolomite)
67 (Nickovic et al., 2012;Journet et al., 2014;Formenti et al., 2014;Scanza et al., 2015;Jeong and
68 Achterberg, 2014). These carbonates are largely insoluble and have very low hygroscopicity

69 (Sullivan et al., 2009;Tang et al., 2016a); however, their reactions with acidic gases in the
70 troposphere can form Ca- and Mg-containing salts with higher hygroscopicity (Sullivan et al.,
71 2009;Tang et al., 2016a;Liu et al., 2008b;Gibson et al., 2006), such as $\text{Ca}(\text{NO}_3)_2$ and $\text{Mg}(\text{NO}_3)_2$.
72 For example, numerous laboratory and field studies have found that due to the formation of
73 $\text{Ca}(\text{NO}_3)_2$ and CaCl_2 from heterogeneous reactions with nitrogen oxides (Li et al., 2010;Tang et
74 al., 2012;Tan et al., 2016;Goodman et al., 2000;Liu et al., 2008a) and HCl (Santschi and Rossi,
75 2006), solid CaCO_3 particles could be converted to aqueous droplets under tropospheric conditions
76 (Krueger et al., 2003;Liu et al., 2008b;Laskin et al., 2005;Tobo et al., 2010;Shi et al., 2008). In
77 addition, MgCl_2 and CaCl_2 are important components in sea salt aerosol (as known as sea spray
78 aerosol). The presence of MgCl_2 and CaCl_2 , in addition to NaCl, can alter the hygroscopicity of
79 sea salt aerosol (Zieger et al., 2017;Gupta et al., 2015); to be more specific, the hygroscopicity of
80 sea salt was found to be significantly smaller than pure NaCl. Furthermore, the CCN activity of
81 saline mineral dust was explored (Gaston et al., 2017), and good correlations were found between
82 the CCN activities of saline mineral dust particles and the abundance of the soluble components
83 (e.g., CaCl_2) they contained.

84 Nevertheless, hygroscopic properties of $\text{Ca}(\text{NO}_3)_2$, $\text{Mg}(\text{NO}_3)_2$, CaCl_2 and MgCl_2 have not
85 been completely understood, especially in the two following aspects. First, hygroscopic growth
86 factors were only measured by one or two previous studies for $\text{Ca}(\text{NO}_3)_2$ (Gibson et al., 2006;Jing
87 et al., 2018), $\text{Mg}(\text{NO}_3)_2$ (Gibson et al., 2006), CaCl_2 (Park et al., 2009) and MgCl_2 aerosols (Park
88 et al., 2009). Considering the importance of these compounds in the troposphere, additional
89 measurements of their hygroscopic growth are clearly warranted. In addition, tropospheric
90 temperatures range from ~200 to ~300 K; however, the effects of temperature on their phase

91 transitions and hygroscopic growth remain largely unclear (Kelly and Wexler, 2005), due to lack
92 of experimental data below room temperature.

93 Small carboxylic acids, such as formic and acetic acids, are abundant in the troposphere
94 (Khare et al., 1999), and previous studies suggested that heterogeneous reactions of mineral dust
95 with formic and acetic acids are efficient (Tong et al., 2010;Ma et al., 2012;Tang et al.,
96 2016b;Hatch et al., 2007;Prince et al., 2008). It was shown that calcium and magnesium acetates
97 were formed in heterogeneous reactions of gaseous acetic acid with MgO and CaCO₃ particles,
98 leading to significant increase in particle hygroscopicity (Ma et al., 2012). However, only a few
99 previous studies explored hygroscopic growth of Mg(CH₃COO)₂ and Ca(CH₃COO)₂, using
100 techniques based on bulk samples (Wang et al., 2005;Pang et al., 2015;Ma et al., 2012). To our
101 knowledge, hygroscopic growth factors have never been reported for Ca(HCOO)₂, Mg(HCOO)₂,
102 Ca(CH₃COO)₂ and Mg(CH₃COO)₂ aerosol particles.

103 To better understand the hygroscopic properties of these Ca- and Mg-containing salts, two
104 complementary techniques were employed in this work to investigate their phase transitions and
105 hygroscopic growth. A vapor sorption analyzer, which measured the sample mass as a function of
106 RH, was used to determine the DRH and solute-to-water ratios for Ca(NO₃)₂·4H₂O,
107 Mg(NO₃)₂·6H₂O, CaCl₂·6H₂O, MgCl₂·6H₂O, Ca(HCOO)₂, Mg(HCOO)₂·2H₂O,
108 Ca(CH₃COO)₂·H₂O and Mg(CH₃COO)₂·4H₂O at different temperatures (5-30 °C). Furthermore,
109 hygroscopic growth factors of Ca(NO₃)₂, Mg(NO₃)₂, CaCl₂, MgCl₂, Ca(HCOO)₂, Mg(HCOO)₂,
110 Ca(CH₃COO)₂ and Mg(CH₃COO)₂ aerosol particles were determined at room temperature up to
111 90% RH, using a humidity-tandem differential mobility analyzer. This work would significantly
112 increase our knowledge in the hygroscopicity of these compounds, hence leading to a better
113 understanding of the physicochemical properties of mineral dust and sea salt aerosols.

114 **2 Experimental section**

115 Hygroscopic growth of Ca- and Mg-containing salts were investigated using two
116 complementary techniques, i.e. a humidity-tandem differential mobility analyzer (H-TDMA) and
117 a vapor sorption analyzer (VSA). Eight salts, all supplied by Aldrich, were investigated in this
118 work, including $\text{Ca}(\text{NO}_3)_2 \cdot 4\text{H}_2\text{O}$ (>99%), $\text{Mg}(\text{NO}_3)_2 \cdot 6\text{H}_2\text{O}$ (99%), $\text{CaCl}_2 \cdot 6\text{H}_2\text{O}$ (>99%),
119 $\text{MgCl}_2 \cdot 6\text{H}_2\text{O}$ (>99%), $\text{Ca}(\text{HCOO})_2$ (>99%), $\text{Mg}(\text{HCOO})_2 \cdot 2\text{H}_2\text{O}$ (98%), $\text{Ca}(\text{CH}_3\text{COO})_2 \cdot \text{H}_2\text{O}$
120 (>99%) and $\text{Mg}(\text{CH}_3\text{COO})_2 \cdot 4\text{H}_2\text{O}$ (99%).

121 **2.1 H-TDMA experiments**

122 H-TDMA measurements were carried out at Institute of Chemistry, Chinese Academy of
123 Sciences, and the experimental setup was detailed in previous work (Peng et al., 2016; Lei et al.,
124 2014). Hygroscopic growth of size-selected aerosol particles was determined by measuring their
125 mobility diameters at different RH. An atomizer (MSP 1500) was used to generate aerosol particles.
126 Solutions used for atomization were prepared using ultrapure water, and their typical
127 concentrations were 0.3-0.4 g L⁻¹. After exiting the atomizer, an aerosol flow (300 mL/min) was
128 passed through a Nafion dryer and then a diffusion dryer filled with silica gel to reach a final RH
129 of <5%. The aerosol flow was then delivered through a neutralizer and the first differential
130 mobility analyzer (DMA) to produce quasi-monodisperse aerosol particles with a mobility
131 diameter of 100 nm. After that, the aerosol flow was transferred through a humidification section
132 with a residence time of ~27 s to be humidified to a given RH. The humidification section was
133 made of two Nafion humidifiers (MD-700-12F-1, Perma Pure) connected in series. The RH of the
134 resulting aerosol flow was monitored using a dew-point meter, which had an absolute uncertainty
135 of ±0.8% in RH measurement as stated by the manufacturer (Michell, UK). After humidification,
136 the size distribution of aerosol particles was measured using a scanning mobility particle sizer

137 (SMPS) which consisted of the second DMA coupled with a condensation particle counter (TSI
138 3776). For the second DMA, the aerosol flow and the sheath flow were always maintained at the
139 same RH. The flow rate ratios of the aerosol flow to the sheath flow were set to 1:10 for both
140 DMA.

141 In our work, the hygroscopic growth factor (GF) is defined as the ratio of measured
142 mobility diameters at a given RH to that at dry conditions:

$$143 \quad GF = \frac{d}{d_0} \quad (1)$$

144 where d_0 and d are the measured mobility diameters at <5% RH and at a given RH, respectively.
145 In our work the dry mobility diameter selected using the first DMA was always 100 nm, and no
146 shape factors were used to correct the dry particle diameters. Size distributions of all the eight
147 types of aerosol particles, measured using the SMPS, were found to be unimode, as illustrated by
148 Figure S1 (in the supplementary information) in which size distributions of $\text{Ca}(\text{NO}_3)_2$ aerosols at
149 4, 50 and 90% RH are displayed as an example. The TDMAinv algorithm (Gysel et al., 2009) was
150 applied to the H-TDMA data.

151 All the experiments were carried out at room temperature (298 ± 1 K), and in each
152 experiment hygroscopic growth of aerosol particles was determined at 12 different RH, i.e. <5, 10,
153 20, 30, 40, 50, 60, 70, 75, 80, 85, and 90%. The absolute uncertainties in RH were estimated to be
154 within $\pm 2\%$. Hygroscopic growth of each compound was measured three times. The performance
155 of the H-TDMA setup was routinely checked by measuring the hygroscopic growth of 100 nm
156 $(\text{NH}_4)_2\text{SO}_4$ and NaCl aerosol particles. Good agreement between measured hygroscopic growth
157 curves with those predicted using the E-AIM model (Clegg et al., 1998) was always found for
158 $(\text{NH}_4)_2\text{SO}_4$ and NaCl aerosols, as detailed in our previous work (Peng et al., 2016; Jing et al., 2016).

159 2.2 VSA experiments

160 The vapor sorption analyzer (Q5000SA), which measured the mass of a bulk sample as a
161 function of RH under isotherm conditions, was manufactured by TA Instruments (New Castle, DE,
162 USA). These experiments were performed at Guangzhou Institute of Geochemistry, Chinese
163 Academy of Sciences, and the instrument and experimental method were described elsewhere (Gu
164 et al., 2017a;Gu et al., 2017b;Jia et al., 2018). Experiments could be conducted in a temperature
165 range of 5-85 °C with an accuracy of ± 0.1 °C and a RH range of 0-98% with an absolute accuracy
166 of $\pm 1\%$. The mass measurement had a range of 0-100 mg, and its sensitivity was stated to be <0.1
167 μg . Initial mass of samples used in an experiment was usually in the range of 0.5-1 mg.

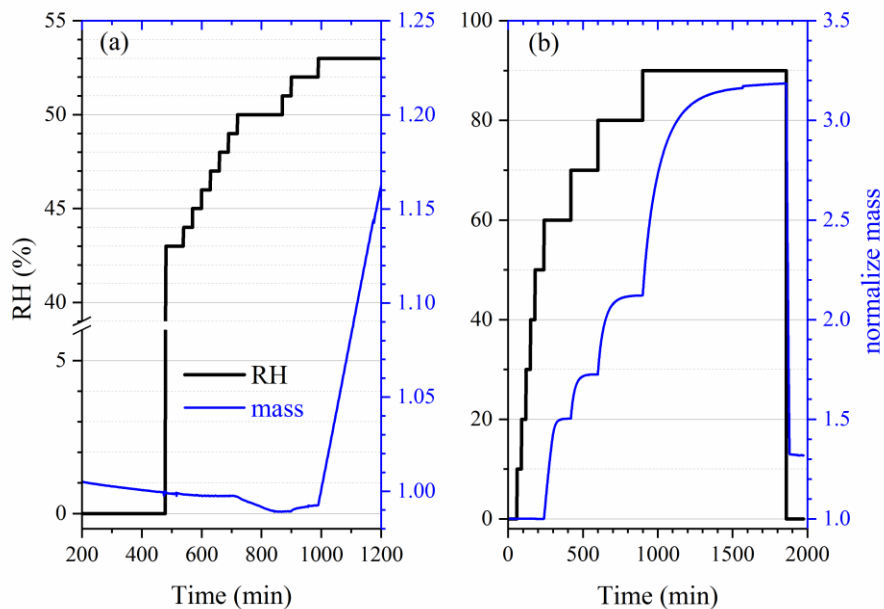
168 Two different types of experiments were carried out. The mass hygroscopic growth was
169 studied in the first type of experiments: after the sample was dried at $<1\%$ RH as a given
170 temperature, RH was increased to 90% stepwise with an increment of 10% per step; after that, RH
171 was set to 0% (the actual RH was measured to be $<1\%$) to dry the sample again. The second type
172 of experiments were conducted to measure DRH values: the sample was first dried at a given
173 temperature, and RH was increased to a value which was at least 5% lower than the expected DRH;
174 RH was then increased stepwise with an increment of 1% until a significant increase in sample
175 mass (when compared to the baseline drift) was observed, and the RH at which the sample mass
176 showed a significant increase was equal to its DRH. Each **experiment** was repeated at least three
177 times, and the average value and standard deviation were reported. At each RH the sample was
178 considered to reach equilibrium with the environment when its mass change was $<0.1\%$ within 30
179 min, and RH was changed to the next value only after the sample mass was stabilized. The time to
180 reach a new equilibrium varied with compounds and largely depended on the dry sample mass, i.e.
181 a sample with larger dry mass would took longer to reach the equilibrium.

182 **3 Results and discussion**

183 **3.1 Hygroscopicity of nitrates and chlorides**

184 **3.1.1 DRH at different temperature**

185 First we investigated the effect of temperature on the DRH of $\text{Ca}(\text{NO}_3)_2 \cdot 4\text{H}_2\text{O}$,
186 $\text{Mg}(\text{NO}_3)_2 \cdot 6\text{H}_2\text{O}$ and $\text{MgCl}_2 \cdot 6\text{H}_2\text{O}$, which are the most stable forms of corresponding salts for the
187 temperature range (5-30 °C) considered in this work (Kelly and Wexler, 2005). Figure 1a shows
188 the change of RH and normalized sample mass as a function of time in an experiment to measure
189 the DRH of $\text{Mg}(\text{NO}_3)_2 \cdot 6\text{H}_2\text{O}$ at 25 °C. Abrupt and significant increase in sample mass was
190 observed when RH was increased from 52 to 53%, suggesting that the deliquescence occurred
191 between 52 and 53% RH. Therefore, its DRH was measured to be 52.5 ± 0.5 %. It should be noted
192 that the mass change was >15% when RH was increased from 52 to 53%, as shown in Figure 1a;
193 such a large mass increase cannot be solely caused by water adsorption, **since the mass of several**
194 **monolayers of adsorbed water is estimated to be <1% of the dry particle mass (Gu et al., 2017b).**
195 The continuous but small decrease in sample mass (about 1% in total) with time (around 500-1000
196 min) before deliquescence took place, as shown in Figure 1a, was likely caused by desorption of
197 residual water contained by the sample under investigation.



198
 199 **Figure 1.** Change of normalized sample mass (blue curve, right y-axis) and RH (black curve, left
 200 y-axis) as a function of time. (a) A typical experiment conducted to measure the DRH; (b) A typical
 201 experiment conducted to measure mass hygroscopic growth factors. In the two experiments shown
 202 here, $\text{Mg}(\text{NO}_3)_2 \cdot 6\text{H}_2\text{O}$ was investigated at 25 °C.

203
 204 Table 1 summarizes our measured DRH of $\text{Ca}(\text{NO}_3)_2 \cdot 4\text{H}_2\text{O}$, $\text{Mg}(\text{NO}_3)_2 \cdot 6\text{H}_2\text{O}$ and
 205 $\text{MgCl}_2 \cdot 6\text{H}_2\text{O}$ as a function of temperature (5-30 °C). DRH values show a strong dependence on
 206 temperature for $\text{Ca}(\text{NO}_3)_2 \cdot 4\text{H}_2\text{O}$ (decreasing from 60.5% at 5 °C to 46.0% at 30 °C) and a weaker
 207 temperature dependence for $\text{Mg}(\text{NO}_3)_2 \cdot 6\text{H}_2\text{O}$ (decreasing from 57.5% at 5 °C to 50.5% at 30 °C);
 208 in contrast, the DRH values of $\text{MgCl}_2 \cdot 6\text{H}_2\text{O}$ (31.5-32.5 %) exhibit little variation with temperature
 209 (5-30 °C). Several previous studies have reported the DRH of $\text{Ca}(\text{NO}_3)_2 \cdot 4\text{H}_2\text{O}$, $\text{Mg}(\text{NO}_3)_2 \cdot 6\text{H}_2\text{O}$
 210 and $\text{MgCl}_2 \cdot 6\text{H}_2\text{O}$, and their results are compared with our work in the following paragraphs.

211

212 **Table 1.** DRH (in %) of $\text{Ca}(\text{NO}_3)_2 \cdot 4\text{H}_2\text{O}$, $\text{Mg}(\text{NO}_3)_2 \cdot 6\text{H}_2\text{O}$ and $\text{MgCl}_2 \cdot 6\text{H}_2\text{O}$ measured in this work
 213 as a function of temperatures (5-30 °C). Solubility data (mol per kg water) compiled by Kelly and
 214 Wexler (2005) was used to calculate solubilities in mol per mol water. All the errors given in this
 215 work are standard deviations.

T (°C)	$\text{Ca}(\text{NO}_3)_2 \cdot 4\text{H}_2\text{O}$	$\text{Mg}(\text{NO}_3)_2 \cdot 6\text{H}_2\text{O}$	$\text{MgCl}_2 \cdot 6\text{H}_2\text{O}$
5	60.5±1.0	57.5±1.0	32.5±1.0
10	58.0±1.0	56.5±1.0	32.5±1.0
15	55.5±1.0	54.5±1.0	32.5±1.0
20	52.5±1.0	53.5±1.0	32.5±1.0
25	49.5±1.0	52.5±1.0	31.5±1.0
30	46.0±1.0	50.5±1.0	31.5±1.0
solubility (mol per kg water)	8.4	4.9	5.84
solubility (A, mol per mol water)	0.1512	0.0882	0.1051
$A \cdot \Delta H_s / R$ (K)	913±59	427±28	--
ΔH_s (kJ mol ⁻¹)	50.2±3.3	40.3±2.6	--

216 The $A \cdot \Delta H_s / R$ and ΔH_s values were not estimated for $\text{MgCl}_2 \cdot 6\text{H}_2\text{O}$ because the difference in its measured
 217 DRH between 5 and 30 °C was very small or even insignificant. Please refer to Section 3.1.1 for further
 218 details.

219
 220 **$\text{Ca}(\text{NO}_3)_2 \cdot 4\text{H}_2\text{O}$:** RH of air in equilibrium with saturated $\text{Ca}(\text{NO}_3)_2 \cdot 4\text{H}_2\text{O}$ solutions, i.e.
 221 the DRH values of $\text{Ca}(\text{NO}_3)_2 \cdot 4\text{H}_2\text{O}$, were measured to be 55.9, 55.4, 50.5 and 46.7% at 15, 20, 25
 222 and 30 °C (Adams and Merz, 1929), and the absolute differences between DRH reported by Adams
 223 and Merz (1929) and those measured in our work are <3%. The water vapor pressures of saturated
 224 $\text{Ca}(\text{NO}_3)_2 \cdot 4\text{H}_2\text{O}$ solutions were measured to be 0.693, 0.920, 1.253, 1.591 and 1.986 kPa at 10, 15,
 225 20, 25 and 30 °C (Apelblat, 1992), corresponding to DRH of 56, 54, 54, 50 and 47%, respectively;
 226 therefore, the absolute difference between DRH measured in our work and those derived from
 227 Apelblat (1992) are <2%. In another study (Al-Abadleh et al., 2003), RH over the saturated

228 $\text{Ca}(\text{NO}_3)_2 \cdot 4\text{H}_2\text{O}$ solution was measured to be $57 \pm 5\%$ at room temperature; in other words, Al-
229 Abadleh et al. (2003) reported a DRH of $57 \pm 5\%$ for $\text{Ca}(\text{NO}_3)_2 \cdot 4\text{H}_2\text{O}$, slightly larger than that
230 ($49.5 \pm 1.0\%$ at $25\text{ }^\circ\text{C}$) determined in our work.

231 **$\text{Mg}(\text{NO}_3)_2 \cdot 6\text{H}_2\text{O}$:** Water vapor pressures of saturated $\text{Mg}(\text{NO}_3)_2 \cdot 6\text{H}_2\text{O}$ solutions were
232 determined to be 0.737, 1.017, 1.390, 1.813 and 2.306 kPa at 10, 15, 20, 25 and $30\text{ }^\circ\text{C}$ (Apelblat,
233 1992), giving DRH of 60, 60, 59, 57 and 54% at corresponding temperatures. The vapor pressure
234 of saturated $\text{Mg}(\text{NO}_3)_2 \cdot 6\text{H}_2\text{O}$ solutions at $25\text{ }^\circ\text{C}$ were reported to be 1.674 and 1.666 kPa by another
235 two studies (Biggs et al., 1955; Robinson and Stokes, 1959), corresponding to DRH of $\sim 53\%$. In
236 addition, the water activity of the saturated $\text{Mg}(\text{NO}_3)_2$ solution was measured to be 0.528 at $25\text{ }^\circ\text{C}$
237 (Rard et al., 2004), also suggesting a DRH value of $\sim 53\%$; similarly, RH over the saturated
238 $\text{Mg}(\text{NO}_3)_2$ solution was reported to be $\sim 53\%$ at $22\text{-}24\text{ }^\circ\text{C}$ (Li et al., 2008b). Al-Abadleh and
239 Grassian (2003) investigated the phase transition of the $\text{Mg}(\text{NO}_3)_2 \cdot 6\text{H}_2\text{O}$ film, and its DRH was
240 determined to be 49-54% at $23\text{ }^\circ\text{C}$. As shown in Table 1, DRH measured in our work agree very
241 well with those reported by most of previous studies (Biggs et al., 1955; Robinson and Stokes,
242 1959; Al-Abadleh and Grassian, 2003; Rard et al., 2004), but are always 3-5% lower than those
243 derived from Apelblat (1992). This may imply that water vapor pressure measurements by
244 Apelblat (1992) could have unknown systematical errors.

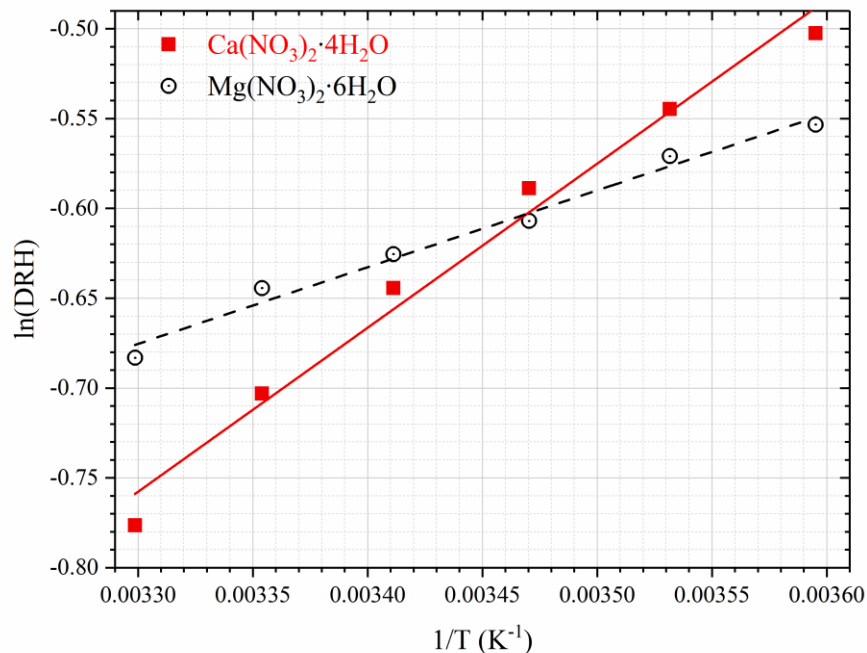
245 **$\text{MgCl}_2 \cdot 6\text{H}_2\text{O}$:** Kelly and Wexler (2005) calculated DRH of $\text{MgCl}_2 \cdot 6\text{H}_2\text{O}$ from vapor
246 pressures of saturated $\text{MgCl}_2 \cdot 6\text{H}_2\text{O}$ solutions measured by previous work, and found that DRH
247 values were in the range of 33-34% for temperatures at $0\text{-}40\text{ }^\circ\text{C}$. In addition, water activity of the
248 saturated MgCl_2 solution was reported to be 0.3278 at $25\text{ }^\circ\text{C}$ (Rard and Miller, 1981),
249 corresponding to a DRH value of $\sim 33\%$ for $\text{MgCl}_2 \cdot 6\text{H}_2\text{O}$. The DRH values of $\text{MgCl}_2 \cdot 6\text{H}_2\text{O}$
250 measured in our work, as summarized in Table 1, show excellent agreement with those reported

251 by previous work (Rard and Miller, 1981; Kelly and Wexler, 2005). Phase transition and
252 deliquescence behavior of $\text{CaCl}_2 \cdot 6\text{H}_2\text{O}$ were also investigated in our work and found to be very
253 complex, and the result will be discussed in Section 3.1.3.

254 Temperature in the troposphere varies from ~ 200 to >300 K, and it is thus warranted to
255 explore the effects of temperature on hygroscopic properties of atmospherically relevant particles.
256 The dependence of DRH on temperature can usually be approximated by the Clausius-Clapeyron
257 equation (Wexler and Seinfeld, 1991; Seinfeld and Pandis, 2016; Jia et al., 2018):

$$258 \quad \ln[\text{DRH}(T)] = \ln[\text{DRH}(298)] + \frac{A \cdot \Delta H_s}{R} \left(\frac{1}{T} - \frac{1}{298} \right) \quad (2)$$

259 where T is temperature (K), $\text{DRH}(T)$ and $\text{DRH}(298)$ are the DRH at T and 298 K, R is the gas
260 constant ($8.314 \text{ J mol}^{-1} \text{ K}^{-1}$), and ΔH_s is the enthalpy of dissolution (J mol^{-1}). The dimensionless
261 constant, A , is numerically equal to the water solubility of the salt under investigation in the unit
262 of mol per mol water. Figure 2 shows the dependence of DRH values on temperature for
263 $\text{Ca}(\text{NO}_3)_2 \cdot 4\text{H}_2\text{O}$ and $\text{Mg}(\text{NO}_3)_2 \cdot 6\text{H}_2\text{O}$, confirming that Eq. (2) can indeed approximate the
264 temperature dependence. The slope, which is equal to $A \cdot \Delta H_s / R$, was determined to be 913 ± 59 K
265 for $\text{Ca}(\text{NO}_3)_2 \cdot 4\text{H}_2\text{O}$ and 427 ± 28 K for $\text{Mg}(\text{NO}_3)_2 \cdot 6\text{H}_2\text{O}$, and thus ΔH_s was derived to be 50.2 ± 3.3
266 kJ mol^{-1} for $\text{Ca}(\text{NO}_3)_2 \cdot 4\text{H}_2\text{O}$ and $40.3 \pm 2.6 \text{ kJ mol}^{-1}$ for $\text{Mg}(\text{NO}_3)_2 \cdot 6\text{H}_2\text{O}$. It should be noted that
267 for Eq. (2) to be valid, both the enthalpy of dissolution and the water solubility are assumed to be
268 constant for the temperature range considered. The variation of DRH with temperature ($5\text{-}30 \text{ }^\circ\text{C}$)
269 was very small and even insignificant for $\text{MgCl}_2 \cdot 6\text{H}_2\text{O}$; as a result, we did not attempt to estimate
270 the ΔH_s values for $\text{MgCl}_2 \cdot 6\text{H}_2\text{O}$ since such estimation would have large errors.



271

272 **Figure 2.** Dependence of DRH on temperature for $\text{Ca}(\text{NO}_3)_2 \cdot 4\text{H}_2\text{O}$ and $\text{Mg}(\text{NO}_3)_2 \cdot 6\text{H}_2\text{O}$.

273 **3.1.2 Water-to-solute ratios as a function of RH**

274 The change of sample mass with RH (0-90%) was measured at 5 and 25 °C for
 275 $\text{Ca}(\text{NO}_3)_2 \cdot 4\text{H}_2\text{O}$, $\text{Mg}(\text{NO}_3)_2 \cdot 6\text{H}_2\text{O}$ and $\text{MgCl}_2 \cdot 6\text{H}_2\text{O}$, using the vapor sorption analyzer. The mass
 276 change, relative to that at 0% RH, can be used to calculate water-to-solute ratios (WSR, defined in
 277 this work as the molar ratio of H_2O to Ca^{2+} or Mg^{2+}) for deliquesced samples. Small **increases** in
 278 m/m_0 (typically <2%) were observed for some compounds (as shown in Tables 2 and 6) when RH
 279 was below corresponding DRH values, mainly due to water adsorption/desorption and baseline
 280 drift. As summarized in Table 2, decrease in temperature would lead to increase in WSR at a given
 281 RH: at 90% RH for example, WSR were determined to be 28.78 ± 0.20 at 25 °C and 31.80 ± 0.96 at
 282 5 °C for $\text{Ca}(\text{NO}_3)_2 \cdot 4\text{H}_2\text{O}$, 36.87 ± 0.23 at 25 °C and 41.40 ± 1.36 at 5 °C for $\text{Mg}(\text{NO}_3)_2 \cdot 6\text{H}_2\text{O}$, and
 283 36.26 ± 1.76 at 25 °C and 39.55 ± 2.43 at 5 °C for $\text{MgCl}_2 \cdot 6\text{H}_2\text{O}$, respectively. As discussed in Section
 284 3.1.1, the enthalpies of dissolution (ΔH_s) are negative for these compounds, suggesting that their

285 dissolution processes in water are exothermic; therefore, dissolution is favored at lower
 286 temperatures and at a given RH, decrease in temperature would lead to increase in WSR in the
 287 aqueous solutions. Several previous studies have measured RH over aqueous $\text{Ca}(\text{NO}_3)_2$, $\text{Mg}(\text{NO}_3)_2$
 288 and MgCl_2 solutions at given concentrations, and their results are compared with our work, as
 289 discussed below.

290
 291 **Table 2.** Mass growth factors (m/m_0 , defined as the ratio of sample mass at a given RH to that at
 292 0% RH) and water-to-solute ratios (WSR) as a function of RH (0-90%) at 25 and 5 °C for
 293 $\text{Ca}(\text{NO}_3)_2 \cdot 4\text{H}_2\text{O}$, $\text{Mg}(\text{NO}_3)_2 \cdot 6\text{H}_2\text{O}$ and $\text{MgCl}_2 \cdot 6\text{H}_2\text{O}$. WSR were only calculated for RH exceeding
 294 the DRH (i.e. when the sample was deliquesced). All the errors given in this work are standard
 295 deviations.

		Ca(NO ₃) ₂ ·4H ₂ O, 25 °C		Ca(NO ₃) ₂ ·4H ₂ O, 5 °C	
RH (%)	m/m_0	WSR	m/m_0	WSR	
0	1.000±0.001	--	1.000±0.001	--	
10	1.000±0.001	--	1.001±0.001	--	
20	1.014±0.005	--	1.005±0.003	--	
30	1.016±0.007	--	1.005±0.002	--	
40	1.017±0.009	--	1.009±0.003	--	
50	1.237±0.006	7.10±0.03	1.032±0.005	--	
60	1.363±0.008	8.76±0.05	1.041±0.002	--	
70	1.550±0.009	11.22±0.06	1.610±0.010	12.00±0.07	
80	1.897±0.012	15.77±0.10	1.979±0.027	16.85±0.23	
90	2.889±0.020	28.78±0.20	3.119±0.095	31.80±0.96	
		Mg(NO ₃) ₂ ·6H ₂ O, 25 °C		Mg(NO ₃) ₂ ·6H ₂ O, 5 °C	
RH (%)	m/m_0	WSR	m/m_0	WSR	
0	1.000±0.001	--	1.000±0.001	--	
10	1.000±0.001	--	1.000±0.001	--	
20	1.000±0.001	--	1.000±0.001	--	

30	1.001±0.001	--	1.000±0.001	--
40	1.001±0.001	--	1.000±0.001	--
50	1.000±0.001	--	1.000±0.001	--
60	1.503±0.001	13.15±0.01	1.539±0.003	13.67±0.03
70	1.724±0.001	16.30±0.01	1.773±0.007	16.99±0.07
80	2.121±0.001	21.94±0.01	2.203±0.021	23.11±0.22
90	3.171±0.029	36.87±0.23	3.489±0.114	41.40±1.36
MgCl ₂ ·6H ₂ O, 25 °C			MgCl ₂ ·6H ₂ O, 5 °C	
RH (%)	<i>m/m</i> ₀	WSR	<i>m/m</i> ₀	WSR
0	1.000±0.001	--	1.000±0.001	--
10	1.000±0.001	--	1.000±0.001	--
20	1.000±0.001	--	1.000±0.001	--
30	1.001±0.001	--	1.000±0.001	--
40	1.344±0.057	9.89±0.42	1.327±0.082	9.69±0.60
50	1.489±0.062	11.52±0.48	1.473±0.090	11.34±0.69
60	1.677±0.072	13.65±0.58	1.667±0.100	13.52±0.82
70	1.951±0.084	16.74±0.72	1.950±0.117	16.72±1.00
80	2.433±0.117	22.18±1.06	2.465±0.148	22.54±1.35
90	3.681±0.178	36.26±1.76	3.972±0.244	39.55±2.43

296

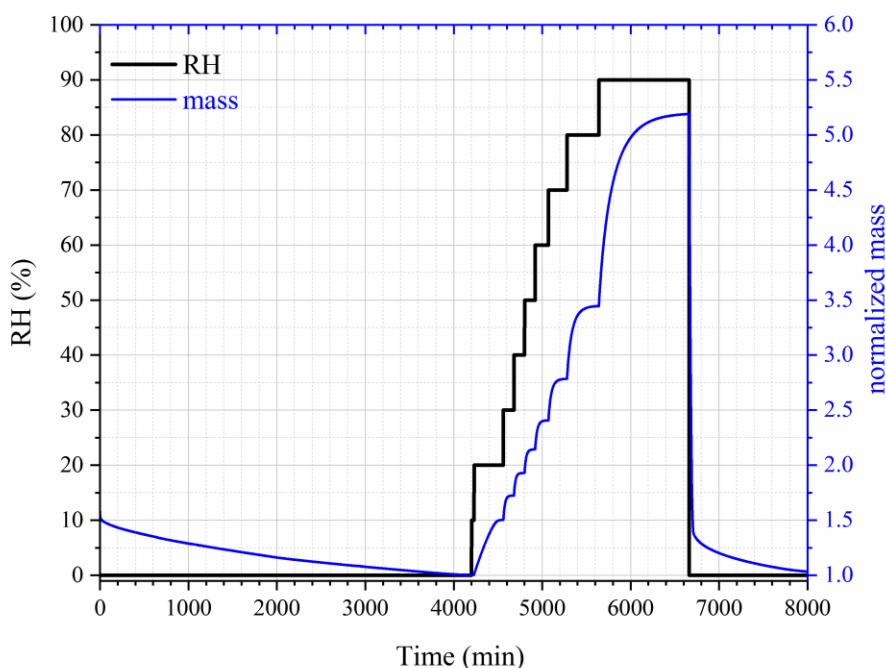
297 **Ca(NO₃)₂:** Water activities of Ca(NO₃)₂ solutions at 25 °C were measured to be 0.904,
298 0.812 and 0.712 when the concentrations were 2.0, 3.5 and 5.0 mol kg⁻¹, respectively (El
299 Guendouzi and Marouani, 2003). Since water activity of a solution is equal to the RH of air in
300 equilibrium with the solution, it can be derived that the molality concentrations of Ca(NO₃)₂
301 solution were 2.0, 3.5 and 5.0 mol kg⁻¹ when RH was **90.4, 81.2 and 71.2%**; in other words, WSR
302 were found to be 11.1, 15.9 and 27.8 at 71.2, 81.2 and 90.4 % RH, respectively (El Guendouzi and
303 Marouani, 2003). As shown in Table 2, in our work WSR were determined to be 11.22±0.06,
304 15.77±0.10 and 28.78±0.20 at 70, 80 and 90% RH for Ca(NO₃)₂ solutions at the same temperature,
305 suggesting good agreement with El Guendouzi and Marouani (2003).

306 **Mg(NO₃)₂:** Water activities of Mg(NO₃)₂ solutions were reported to be 0.897, 0.812 and
307 0.702 when the concentrations of the bulk solutions were 1.6, 2.5 and 3.5 mol kg⁻¹ at 25 °C,
308 respectively (Rard et al., 2004); this means that WSR were equal to 15.9, 22.2 and 34.7 at 70.2,
309 81.2 and 89.7% RH. Ha and Chan (1999) fitted their measured water activities of Mg(NO₃)₂ as a
310 function of molality concentration at 20-24 °C with a polynomial equation, and WSR were derived
311 to be 12.93, 16.12, 21.50 and 36.09 at 60, 70, 80 and 90% RH. As shown in Table 2, WSR were
312 measured to be 13.15±0.01, 16.30±0.01, 21.94±0.01 and 36.87±0.23 at 60, 70, 80 and 90% RH
313 for deliquesced Mg(NO₃)₂ at 25 °C. Therefore, it can be concluded that for WSR of Mg(NO₃)₂
314 solutions at ~25 °C, our work shows good agreement with the two previous studies (Ha and Chan,
315 1999;Rard et al., 2004).

316 **MgCl₂:** Water activities of MgCl₂ solutions were reported to be 0.909, 0.800, 0.692, 0.491
317 and 0.408 when the concentrations were 1.4, 2.4, 3.2, 4.6 and 5.2 mol kg⁻¹ (Rard and Miller, 1981),
318 i.e. WSR were equal to 10.7, 12.1, 17.4, 23.1 and 39.7 at 40.8, 49.1, 69.2, 80.0 and 90.9% RH. In
319 another work (Ha and Chan, 1999), an electrodynamic balance was used to investigate
320 hygroscopic growth of MgCl₂ particles at 20-24 °C, and the measured molality concentrations of
321 MgCl₂ solutions as a function of water activity were fitted by a polynomial equation; it can be
322 derived from Ha and Chen (1999) that WSR were equal to 10.65, 12.34, 14.29, 17.04, 22.24 and
323 34.78 when RH were 40, 50, 60, 70, 80 and 90%, respectively. WSR measured in our work, as
324 listed in Table 2, are 9.89±0.42, 11.52±0.48, 16.77±0.072, 16.74±0.72, 22.18±1.06 and 36.26±1.76
325 at 40, 50, 60, 70, 80 and 90% RH. As a result, our work agrees well with the two previous studies
326 (Ha and Chan, 1999;Rard and Miller, 1981) for WSR of MgCl₂ solutions as a function of RH at
327 ~25 °C.

328 **3.1.3 Phase transition of CaCl₂·xH₂O**

329 The change in sample mass of $\text{CaCl}_2 \cdot 6\text{H}_2\text{O}$ with RH was also investigated at 25 °C. As
330 shown in Figure 3, when dried at 0% RH, the sample mass was reduced by 1/3 (from ~1.5 to ~1.0),
331 and it is speculated that $\text{CaCl}_2 \cdot 6\text{H}_2\text{O}$ was converted to $\text{CaCl}_2 \cdot 2\text{H}_2\text{O}$. When RH was increased to
332 10%, no significant increase in sample mass was observed. As RH was further increased to 20%,
333 the sample mass was increased by 48 ± 7 %; this may indicate that $\text{CaCl}_2 \cdot 2\text{H}_2\text{O}$ was converted to
334 $\text{CaCl}_2 \cdot 6\text{H}_2\text{O}$, as the ratio of molar mass of $\text{CaCl}_2 \cdot 6\text{H}_2\text{O}$ (219 g mol^{-1}) to $\text{CaCl}_2 \cdot 2\text{H}_2\text{O}$ (147 g mol^{-1})
335 is 1.49, approximately equal to the ratio of sample mass at 20% RH to that at 10% RH. Further
336 increase in RH to 30% would lead to additional increase in sample mass, implying the
337 deliquescence of the sample and the formation of an aqueous CaCl_2 solution.



338
339 **Figure 3.** Change of normalized sample mass (blue curve, right y-axis) and RH (black curve, left
340 y-axis) as a function of time for $\text{CaCl}_2 \cdot x\text{H}_2\text{O}$ at 25 °C.

341

342 Assuming that $\text{CaCl}_2 \cdot 6\text{H}_2\text{O}$ was converted to $\text{CaCl}_2 \cdot 2\text{H}_2\text{O}$ after being dried at 0% RH, we
 343 could use the change of sample mass as a function of RH to calculate WSR (defined as molar ratio
 344 of H_2O to Ca^{2+}), and the results are listed in Table 3. Please note that we did not calculate WSR at
 345 20% RH, since it is speculated that the significant mass increase at 20% RH was caused by the
 346 transformation of $\text{CaCl}_2 \cdot 2\text{H}_2\text{O}$ to $\text{CaCl}_2 \cdot 6\text{H}_2\text{O}$, as mentioned above. Water activities of aqueous
 347 CaCl_2 solutions as a function of molality concentration reported in a previous study (Rard et al.,
 348 1977) were used to calculate WSR as a function of RH, and the results are also included in Table
 349 3 for comparison. As evident from Table 3, at same/similar RH, WSR measured in our work are
 350 in good agreement with those derived from Rard et al. (1977), supporting our assertion that
 351 $\text{CaCl}_2 \cdot 6\text{H}_2\text{O}$ was converted to $\text{CaCl}_2 \cdot 2\text{H}_2\text{O}$ after being dried at 0% RH. In fact, theoretical
 352 calculations (Kelly and Wexler, 2005) and experimental measurements (Gough et al., 2016) both
 353 suggested that when RH is gradually increased, solid-solid phase transition from $\text{CaCl}_2 \cdot 2\text{H}_2\text{O}$ to
 354 $\text{CaCl}_2 \cdot 6\text{H}_2\text{O}$ would occur before deliquescence takes place.

355
 356 **Table 3.** Mass growth factors (m/m_0 , defined as the ratio of sample mass at a given RH to that at
 357 0% RH) and water-to-solute ratios (WSR) as a function of RH (0-90%) at 25 °C for $\text{CaCl}_2 \cdot x\text{H}_2\text{O}$.
 358 WSR derived from RH over aqueous CaCl_2 solutions as a function of concentration (mol kg^{-1}) at
 359 25 °C (Rard et al., 1977) are also included for comparison. All the errors given in this work are
 360 standard deviations.

our work			Rard et al., 1977		
RH (%)	m/m_0	WSR	RH (%)	molality	WSR
0	1.000±0.001	--	--	--	--
10	1.000±0.001	--	--	--	--
20	1.448±0.072	--	--	--	--
30	1.724±0.007	7.97±0.03	31.2	7.0	7.94

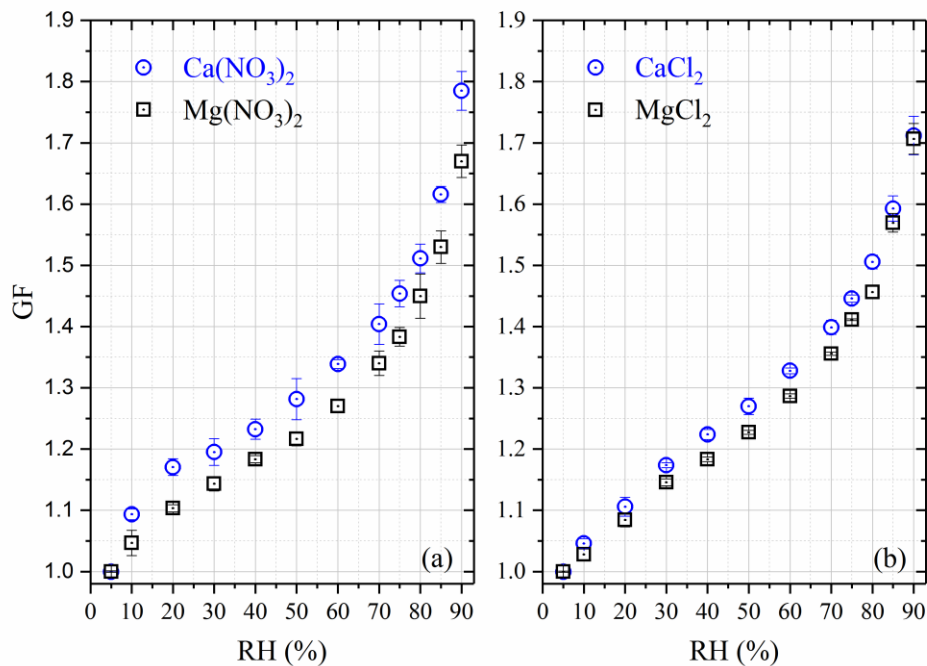
40	1.929±0.008	9.64±0.04	39.2	6.0	9.26
50	2.144±0.010	11.40±0.05	49.9	5.0	11.11
60	2.408±0.012	13.55±0.07	--	--	--
70	2.786±0.015	16.64±0.09	70.1	3.4	16.34
80	3.448±0.020	22.05±0.13	79.8	2.6	21.37
90	5.194±0.030	36.30±0.21	89.9	1.6	37.72

361

362 Additional experiments, in which RH was stepwise increased from 0% with an increment
363 of 1% per step, were carried out in attempt to measure the DRH of $\text{CaCl}_2 \cdot x\text{H}_2\text{O}$ at 25 °C. In all of
364 these experiments, $\text{CaCl}_2 \cdot 6\text{H}_2\text{O}$ was always transformed to $\text{CaCl}_2 \cdot 2\text{H}_2\text{O}$ after being dried at 0%
365 RH. In some of these experiments the deliquescence took place at RH of ~28.5%, which is
366 consistent with the DRH of $\text{CaCl}_2 \cdot 6\text{H}_2\text{O}$ reported in the literature (Kelly and Wexler, 2005),
367 suggesting that $\text{CaCl}_2 \cdot 2\text{H}_2\text{O}$ was first transformed to $\text{CaCl}_2 \cdot 6\text{H}_2\text{O}$ prior to deliquescence; however,
368 in some experiments the deliquescence occurred at RH of ~18.5%, corresponding to the DRH of
369 $\text{CaCl}_2 \cdot 2\text{H}_2\text{O}$ reported previously (Kelly and Wexler, 2005), implying that $\text{CaCl}_2 \cdot 2\text{H}_2\text{O}$ was
370 deliquesced without being transformed to $\text{CaCl}_2 \cdot 6\text{H}_2\text{O}$. The dual deliquescence processes, i.e. 1)
371 transformation of $\text{CaCl}_2 \cdot 2\text{H}_2\text{O}$ to $\text{CaCl}_2 \cdot 6\text{H}_2\text{O}$ prior to deliquescence and 2) direct deliquescence
372 of $\text{CaCl}_2 \cdot 2\text{H}_2\text{O}$, were also observed using Raman spectroscopy at low temperatures (223-273 K)
373 (Gough et al., 2016). It seems that the competition of these two mechanisms are both
374 thermodynamically and kinetically dependent. Since phase transitions of CaCl_2 are not only
375 important for atmospheric aerosols but may also play a role in the existence of liquid water in some
376 hyperarid environments (Gough et al., 2016), further investigation is being carried out by
377 combining the vapor sorption analyzer technique with vibrational spectroscopy.

378 3.1.4 Hygroscopic growth of aerosol particles

379 Hygroscopic growth factors (GF), which were measured using H-TDMA at room
 380 temperature, are displayed in Figure 4 for $\text{Ca}(\text{NO}_3)_2$, CaCl_2 , $\text{Mg}(\text{NO}_3)_2$ and MgCl_2 aerosols, and
 381 the results are also compiled in Table 4. It was found in our work that all the four types of aerosols
 382 exhibit high hygroscopicity, with GF at 90% RH being around 1.7 or larger. In addition, all the
 383 four types of aerosol particles, instead of having distinct solid-liquid phase transitions, showed
 384 significant hygroscopic growth at very low RH (as low as 10%), and their GF increased
 385 continuously with RH. This phenomenon is due to the fact that these aerosol particles, generated
 386 by drying aqueous droplets, were likely to be amorphous. It was also observed in previous work
 387 that some types of particles generated by drying aqueous droplets would be amorphous, such as
 388 $\text{Ca}(\text{NO}_3)_2$ (Gibson et al., 2006;Jing et al., 2018;Tang and Fung, 1997), $\text{Mg}(\text{NO}_3)_2$ (Gibson et al.,
 389 2006;Zhang et al., 2004;Li et al., 2008a), CaCl_2 (Park et al., 2009;Tobo et al., 2009) and MgCl_2
 390 (Cziczo and Abbatt, 2000;Park et al., 2009).



391
 392 **Figure 4.** Hygroscopic growth factors (GF) of aerosol particles as a function of RH measured
 393 using H-TDMA. (a): $\text{Ca}(\text{NO}_3)_2$ and $\text{Mg}(\text{NO}_3)_2$; (b) CaCl_2 and MgCl_2 .

394

395 **Ca(NO₃)₂ and Mg(NO₃)₂ aerosols:** Two previous studies (Jing et al., 2018;Gibson et al.,
396 2006) employed H-TDMA to examine the hygroscopic growth of 100 nm Ca(NO₃)₂ aerosol
397 particles at room temperature. GF were determined to be 1.51 at 80% RH and ~1.77 at 85% RH
398 by Gibson et al. (2008). It should be pointed out that though the DMA-selected dry particle
399 diameters were 100 nm for Ca(NO₃)₂ and Mg(NO₃)₂ aerosols, the dry diameters used by Gibson
400 et al. (2006) were 89 nm for Ca(NO₃)₂ and 77 nm for Mg(NO₃)₂, being extrapolated to 0% RH
401 using the theoretical growth curve based on the Köhler theory. The Köhler theory is based on
402 assumption of solution ideality, and thus may not be applicable to highly concentrated aerosol
403 droplets at very low RH (Seinfeld and Pandis, 2016). If the dry diameter selected using the DMA
404 (i.e. 100 nm) was used in GF calculation, GF reported by Gibson et al. (2006) would be ~1.34 at
405 80% RH and ~1.58 at 85% RH; compared with our results (1.51±0.02 at 80% RH and 1.62±0.01
406 at 85% RH), GF reported by Gibson et al. (2006) are ~11% smaller at 80% RH and only ~3%
407 smaller at 85%. In the second study (Jing et al., 2018), GF were determined to be 1.56 at 80% RH
408 and 1.89 at 90% RH; compared with our results (1.51±0.02 at 80% RH and 1.79±0.03 at 90% RH),
409 GF reported by Jing et al. (2018) were ~3% larger at 80% RH and ~6% larger at 90% RH. Overall,
410 our results show reasonably good agreement with the two previous studies (Gibson et al.,
411 2006;Jing et al., 2018).

412

413 **Table 4.** Hygroscopic growth factors (GF) of Ca(NO₃)₂, CaCl₂, Mg(NO₃)₂ and MgCl₂ aerosol
414 particles measured at room temperature using H-TDMA. The absolute uncertainties in RH were
415 estimated to be within ±2%. All the errors given in this work are standard deviations.

RH (%)	Ca(NO ₃) ₂	CaCl ₂	Mg(NO ₃) ₂	MgCl ₂
--------	-----------------------------------	-------------------	-----------------------------------	-------------------

<5	1.00±0.01	1.00±0.01	1.00±0.01	1.00±0.01
10	1.09±0.01	1.05±0.01	1.05±0.02	1.03±0.01
20	1.17±0.02	1.11±0.02	1.10±0.01	1.08±0.01
30	1.20±0.02	1.17±0.01	1.41±0.01	1.15±0.01
40	1.23±0.02	1.22±0.01	1.18±0.01	1.18±0.01
50	1.28±0.03	1.27±0.01	1.22±0.01	1.23±0.01
60	1.34±0.01	1.33±0.01	1.27±0.01	1.29±0.01
70	1.40±0.03	1.40±0.01	1.34±0.02	1.36±0.01
75	1.45±0.02	1.45±0.01	1.38±0.02	1.41±0.01
80	1.51±0.02	1.51±0.01	1.45±0.04	1.46±0.01
85	1.62±0.01	1.59±0.02	1.53±0.03	1.57±0.02
90	1.79±0.03	1.71±0.03	1.67±0.03	1.71±0.03

416

417 To our knowledge, only one previous study investigated the hygroscopic growth of
418 $\text{Mg}(\text{NO}_3)_2$ aerosol (100 nm) using the H-TDMA (Gibson et al., 2006), and GF was measured to
419 be 1.94 ± 0.02 at 83% RH. As stated above, the theoretical extrapolated diameter (77 nm) at 0%
420 RH, instead of the dry diameter (100 nm) selected using the DMA, were used as the dry diameter
421 to calculate their reported GF (Gibson et al., 2006). If the DMA-selected dry diameter (100 nm)
422 was used in calculation, the GF reported by Gibson et al. (2006) would be ~ 1.49 at 83% RH; for
423 comparison, in our work GF were determined to be 1.45 ± 0.04 and 1.53 ± 0.03 at 80 and 85% RH,
424 suggesting good agreement between the two studies if the DMA-selected dry diameter was used
425 to calculate GF reported by Gibson et al. (2006).

426 **CaCl₂ and MgCl₂ aerosols:** Hygroscopic growth of CaCl₂ and MgCl₂ aerosol particles
427 was explored using a H-TDMA (Park et al., 2009), and as far as we know, this was the only study
428 which reported the H-TDMA measured hygroscopic growth factors of the two aerosols. Three dry
429 diameters (20, 30 and 50 nm) were used for CaCl₂ and MgCl₂ aerosol particles (Park et al., 2009),
430 and no significant size dependence of their hygroscopic properties was observed. GF were

431 measured to be around 1.27, 1.38, 1.48 and 1.59 at 60, 75, 80 and 90 % RH for CaCl₂ (Park et al.,
432 2009). For comparison, GF were determined **in this work** to be 1.33±0.01, 1.45±0.01, 1.51±0.01
433 and 1.71±0.03 at 60, 75, 80 and 90 %, slightly larger than those reported by Park et al. (2009), and
434 the differences were found to be <7%.

435 At 50, 70, 80, 85 and 90% RH, GF of MgCl₂ aerosol were measured to be about 1.17, 1.29,
436 1.47, 1.59 and 1.79 by Park et al. (2009); **for comparison, GF were determined to be** 1.23±0.01,
437 1.36±0.01, 1.46±0.01, 1.57±0.02 and 1.71±0.03 in our work **at the same RHs**. The differences did
438 not exceed 6%, suggesting good agreement between the two studies. Microscopy was used to
439 investigate the hygroscopic growth of micrometer-size MgCl₂ particles deposited on substrates
440 (Gupta et al., 2015), and the ratios of 2-D particle areas, relative to that at <5% RH, were measured
441 to be around 1.65, 1.92, 2.02 and 2.28 at 60, 70, 75 and 80% RH, corresponding to diameter-based
442 GF of approximately 1.28, 1.38, 1.42 and 1.51, respectively. GF of MgCl₂ aerosol, as shown in
443 Table 4, were determined to be 1.29±0.01, 1.36±0.01, 1.41±0.01 and 1.46±0.01 at 60, 70, 75 and
444 80% RH in our work; therefore, the differences between GF reported in our work and those
445 measured by Gupta et al. (2015) were <4%.

446 **Comparison between hygroscopic growth with CCN activities:** GF measured using H-
447 TDMA can be used to calculate the single hygroscopicity parameter, κ_{gf} , using Eq. (3a) (Petters
448 and Kreidenweis, 2007; Tang et al., 2016a; Kreidenweis and Asa-Awuku, 2014):

449
$$\frac{RH}{\exp\left(\frac{A}{d_0 \cdot GF}\right)} = \frac{GF^3 - 1}{GF^3 - (1 - \kappa_{gf})} \quad (3a)$$

450 where GF is the growth factor at a given RH; A is a constant which describes the Kelvin effect and
451 is equal to 2.1 nm for a surface tension of 0.072 J m⁻² (pure water) and temperature of 298.15 K
452 (Tang et al., 2016a). For a dry particle diameter (d_0) of 100 nm, the denominator in the left term

453 of Eq. (3a) is not larger than 1.02; therefore, the Kelvin effect is negligible and Eq. (3a) can be
454 simplified to Eq. (3b):

$$455 \quad RH = \frac{GF^3 - 1}{GF^3 - (1 - \kappa_{gf})} \quad (3b)$$

456 Eq. (4) can be derived by rearranging Eq. (3b):

$$457 \quad \kappa_{gf} = (GF^3 - 1) \frac{1 - RH}{RH} \quad (4)$$

458 In our work, GF data at 90% RH were used to derive κ_{gf} , as usually done in many previous studies
459 (Kreidenweis and Asa-Awuku, 2014). The single hygroscopicity parameter, κ_{ccn} , can also be
460 derived from experimental measurements or theoretical calculations of CCN activities (Petters and
461 Kreidenweis, 2007; Kreidenweis and Asa-Awuku, 2014). Ideally aerosol-water interactions under
462 both subsaturation and supersaturation can be described by a constant single hygroscopicity
463 parameter (Petters and Kreidenweis, 2007). Nevertheless, agreement and discrepancies between
464 growth factors derived and CCN activity derived κ have been reported (Petters and Kreidenweis,
465 2007; Wex et al., 2009; Petters et al., 2009), and several factors can contribute to such discrepancies.
466 First of all, the solutions may not be ideal, and especially aerosol particles under subsaturation may
467 consist of concentrated solutions; secondly, some of the compounds may have limited solubilities.
468 As discussed previously (Petters and Kreidenweis, 2007; Prenni et al., 2007), both factors would
469 lead to lower κ_{gf} , compared to κ_{ccn} . The effect of reduced surface tension, compared to pure water,
470 should be negligible for the eight types of aerosol particles considered in our work, since none of
471 the compounds are known to be surface-active.

472 Comparison between κ_{gf} determined in our work and κ_{ccn} measured in previous studies is
473 summarized in Table 5 and discussed below for $\text{Ca}(\text{NO}_3)_2$, CaCl_2 , $\text{Mg}(\text{NO}_3)_2$ and MgCl_2 aerosols.
474 In previous work which measured CCN activities (Gaston et al., 2017; Sullivan et al., 2009; Tang

475 et al., 2015), the dry particle diameters used were typically in the range of 50-125 nm. The
 476 uncertainties in our derived κ_{gf} have taken into account the uncertainties in measured GF at 90%
 477 RH.

478

479 **Table 5.** Comparison between κ_{gf} measured in our work and κ_{ccn} measured in previous studies.

aerosol	κ_{gf} (this work)	κ_{ccn} (previous studies)
Ca(NO ₃) ₂	0.49-0.56	0.44-0.64 (Sullivan et al., 2009) 0.57-0.59 (Tang et al., 2015)
Mg(NO ₃) ₂	0.38-0.43	not measured yet
CaCl ₂	0.42-0.47	0.46-0.58 (Sullivan et al, 2009) 0.51-0.54 (Tang et al, 2015)) 0.549-0.561 (Gaston et al., 2017)
MgCl ₂	0.42-0.47	0.456-0.464 (Gaston et al., 2017)
Ca(HCOO) ₂	0.28-0.31	0.47-0.52 (Tang et al., 2015)
Mg(HCOO) ₂	0.40-0.45	not measured yet
Ca(CH ₃ COO) ₂	0.09-0.13	0.37-0.47 (Tang et al., 2015)
Mg(CH ₃ COO) ₂	0.28-0.29	not measured yet

480

481 1) For Ca(NO₃)₂ aerosol, κ_{ccn} were measured to be 0.44-0.64 by Sullivan et al. (2009) and
 482 0.57-0.59 by Tang et al. (2015); in our work GF at 90% RH was measured to be 1.79 ± 0.03 , giving
 483 κ_{gf} of 0.49-0.56, in good agreement with κ_{ccn} reported by the two previous studies (Sullivan et al.,
 484 2009; Tang et al., 2015).

485 2) For CaCl₂ aerosol, κ_{ccn} were measured to be 0.46-0.58 by Sullivan et al. (2009), 0.51-
 486 0.54 by Tang et al. (2015), and 0.549-0.561 by Gaston et al. (2017). GF at 90% RH was determined
 487 to be 1.71 ± 0.03 in present work, giving κ_{gf} of 0.42-0.47, slightly lower than κ_{ccn} values measured
 488 previously (Sullivan et al., 2009; Tang et al., 2015; Gaston et al., 2017).

489 3) In our work, GF was determined to be 1.71 ± 0.03 for MgCl_2 at 90% RH, giving κ_{gf} of
490 0.42-0.47; a previous study (Gaston et al., 2017) measured the CCN activity of MgCl_2 aerosol, and
491 κ_{ccn} were determined to be 0.456-0.464, in good agreement with κ_{gf} measured in our work.

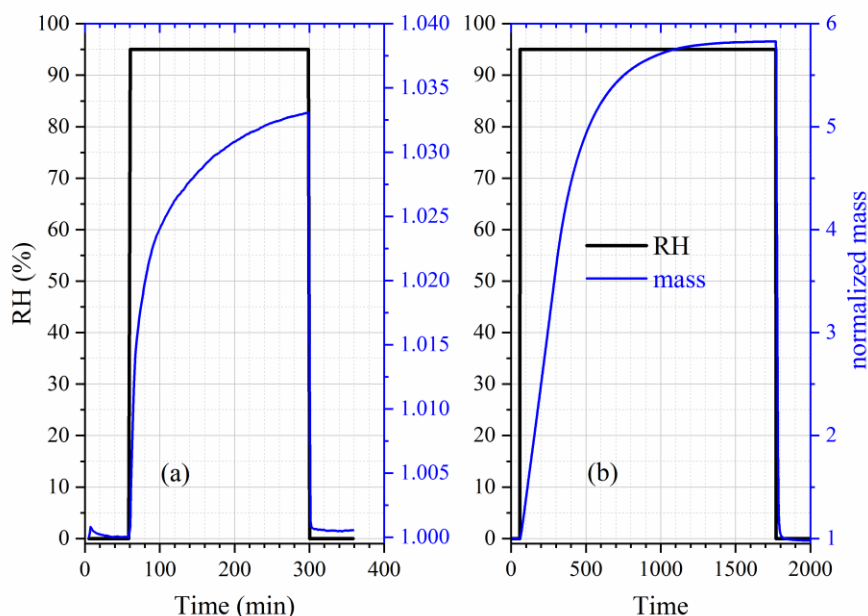
492 4) For $\text{Mg}(\text{NO}_3)_2$ aerosol, GF and κ_{gf} were determined in our work to be 1.67 ± 0.03 and
493 0.38-0.43, respectively. To our knowledge, CCN activities of $\text{Mg}(\text{NO}_3)_2$ aerosol have not been
494 experimentally explored yet, and κ_{ccn} were predicted to be 0.8 for $\text{Mg}(\text{NO}_3)_2$ and 0.3 for
495 $\text{Mg}(\text{NO}_3)_2 \cdot 6\text{H}_2\text{O}$ (Kelly et al., 2007; Kreidenweis and Asa-Awuku, 2014), exhibiting a large
496 variation for the same compound with different hydrate states under dry conditions. These
497 calculations were performed using the Köhler theory, assuming solution ideality (Kelly et al.,
498 2007). As Kelly et al. (2007) pointed out, the hydration states, which are not entirely clear for
499 $\text{Mg}(\text{NO}_3)_2$ aerosol particles under atmospherically relevant conditions, can have large impacts on
500 their hygroscopicity and CCN activities.

501 **3.2 Hygroscopicity of formates and acetates**

502 **3.2.1 DRH and water-to-solute ratios**

503 We measured the mass change of $\text{Ca}(\text{HCOO})_2$, $\text{Mg}(\text{HCOO})_2 \cdot 2\text{H}_2\text{O}$ and
504 $\text{Ca}(\text{CH}_3\text{COO})_2 \cdot \text{H}_2\text{O}$ samples as a function of RH at 25 °C, and found that the sample mass
505 remained essentially constant for all the three compounds when RH was increased from 0 to 90%.
506 Therefore, a series of experiments in which RH was increased to 95% were conducted, and for
507 each compounds three duplicate experiments were carried out. As shown in Figure 5a, when RH
508 was increased from 0 to 95%, a significant while small increase in sample mass (>3%) was
509 observed for $\text{Ca}(\text{HCOO})_2$. The average ratio of sample mass at 95% RH to that at 0% RH was
510 determined to be for 1.043 ± 0.018 for $\text{Ca}(\text{HCOO})_2$ and 1.028 ± 0.008 for $\text{Mg}(\text{HCOO})_2 \cdot 2\text{H}_2\text{O}$ (not

511 shown in Figure 5), probably indicating that the DRH values were >95% for both compounds at
512 25 °C.



513
514 **Figure 5.** Change of normalized sample mass (blue curve, right y-axis) and RH (black curve, left
515 y-axis) as a function of time at 25 °C. (a) Ca(HCOO)₂; (b) Ca(CH₃COO)₂·H₂O.

516
517 When RH was increased from 0 to 95%, large increase in sample mass (almost by a factor
518 of 6), as shown in Figure 6b, was observed for Ca(CH₃COO)₂·H₂O. On average, the ratio of sample
519 mass at 95% RH to that at 0% RH was measured to be 5.849±0.064, corresponding to a WSR
520 (defined as the molar ratio of H₂O to Ca²⁺) of 48.42±0.53 for the aqueous Ca(CH₃COO)₂ solution
521 at 95% RH. This observation suggested that the deliquescence of Ca(CH₃COO)₂·H₂O at 25 °C
522 occurred between 90 and 95% RH. In further experiments significant increase in sample mass
523 (by >10%, and the sample was still increasing sharply when the experiment was terminated) was
524 observed when RH was increased from 90 to 91% for Ca(CH₃COO)₂·H₂O at 25 °C, suggesting
525 giving a measured DRH of 90.5±1.0 %. The DRH of Ca(CH₃COO)₂ and internally mixed

526 $\text{CaCO}_3/\text{Ca}(\text{CH}_3\text{COO})_2$ particles were measured to be 85 and 88% at 5 °C (Ma et al., 2012), using
 527 a modified physisorption analyzer. Since in these two studies DRH were measured at different
 528 temperatures (25 °C in our work and 5 °C by Ma et al.) and the absolute difference in reported
 529 DRH was ~5%, the agreement in reported DRH can be considered to be quite good for
 530 $\text{Ca}(\text{CH}_3\text{COO})_2$.

531 Table 6 summarizes the ratios of sample mass at a given RH to that at 0% RH for
 532 $\text{Mg}(\text{CH}_3\text{COO})_2 \cdot 4\text{H}_2\text{O}$ as a function of RH at 25°C. Being different from $\text{Ca}(\text{HCOO})_2$,
 533 $\text{Mg}(\text{HCOO})_2 \cdot 2\text{H}_2\text{O}$ and $\text{Ca}(\text{CH}_3\text{COO})_2 \cdot \text{H}_2\text{O}$, large increase in sample mass was observed for
 534 $\text{Mg}(\text{CH}_3\text{COO})_2 \cdot 4\text{H}_2\text{O}$ when RH was increased from 70 to 80%. This observation suggested that
 535 the deliquescence of $\text{Mg}(\text{CH}_3\text{COO})_2 \cdot 4\text{H}_2\text{O}$ occurred between 70 and 80% RH. Further
 536 experiments were carried out to measure its DRH: significant increase in sample mass occurred
 537 when RH was increased from 71 to 72%, giving a measured DRH of $71.5 \pm 1.0\%$ at 25 °C. The RH
 538 over the saturated $\text{Mg}(\text{CH}_3\text{COO})_2$ solution at ~23 °C was measured to be 65% (Wang et al., 2005),
 539 slightly lower than the DRH determined in our work.

540

541 **Table 6.** Mass growth factors (m/m_0 , defined as the ratios of sample mass at a given RH to that at
 542 0% RH) and water-to-solute ratios (WSR) as a function of RH (0-90%) at 25 °C for
 543 $\text{Mg}(\text{CH}_3\text{COO})_2 \cdot 4\text{H}_2\text{O}$. WSR are only calculated for RH exceeding the DRH (i.e. when the sample
 544 was deliquesced). All the errors given in this work are standard deviations.

RH (%)	0	10	20	30	40
m/m_0	1.000 ± 0.001	1.012 ± 0.021	1.012 ± 0.022	1.013 ± 0.022	1.013 ± 0.022
WSR	--	--	--	--	--
RH (%)	50	60	70	80	90
m/m_0	1.014 ± 0.023	1.015 ± 0.025	1.033 ± 0.031	2.029 ± 0.013	3.100 ± 0.021
WSR	--	--	--	16.24 ± 0.11	28.97 ± 0.20

545

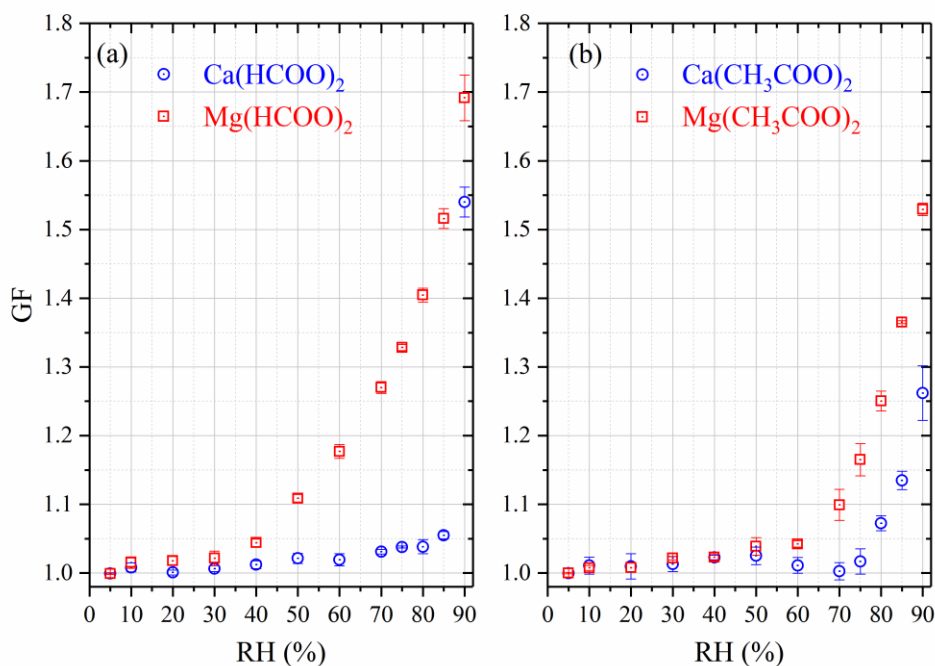
546 The ratios of sample mass, relative to that at 0% RH, were measured to be 2.029 ± 0.013
547 and 3.100 ± 0.021 at 80 and 90% RH, corresponding to WSR of 16.24 ± 0.11 at 80% RH and
548 28.97 ± 0.20 at 90% RH for aqueous $\text{Mg}(\text{CH}_3\text{COO})_2$ solutions. A electrodynamic balance coupled
549 to Raman spectroscopy was employed to study the hygroscopic growth of $\text{Mg}(\text{CH}_3\text{COO})_2$ at ~ 23
550 $^\circ\text{C}$ (Wang et al., 2005), and WSR was determined to be ~ 15.6 at 80% RH, in good agreement with
551 our work. Ma et al. (2012) found that after heterogeneous reaction with $\text{CH}_3\text{COOH}(\text{g})$ at 50% RH
552 for 12 h, the hygroscopicity of MgO particles, which was initially rather non-hygroscopic, was
553 substantially increased due to the formation of $\text{Mg}(\text{CH}_3\text{COO})_2$. The conclusion drawn by Ma et al.
554 (2012) is qualitatively consistent with the results obtained in our work.

555 Table 5 also reveals that a small increase in sample mass (by $\sim 3\%$, relative to that at 0%
556 RH) was observed for $\text{Mg}(\text{CH}_3\text{COO})_2 \cdot 4\text{H}_2\text{O}$ when RH was increased to 70% before the
557 deliquescence of $\text{Mg}(\text{CH}_3\text{COO})_2 \cdot 4\text{H}_2\text{O}$ took place. This could be due to the possibility that
558 $\text{Mg}(\text{CH}_3\text{COO})_2 \cdot 4\text{H}_2\text{O}$ samples used in our work may contain a small fraction of amorphous
559 $\text{Mg}(\text{CH}_3\text{COO})_2$, which would take up some amount of water at RH below the DRH of
560 $\text{Mg}(\text{CH}_3\text{COO})_2 \cdot 4\text{H}_2\text{O}$ (Pang et al., 2015; Wang et al., 2005).

561 **3.2.2 Hygroscopic growth of aerosol particles**

562 Figure 6 and Table 6 display hygroscopic growth factors of $\text{Ca}(\text{HCOO})_2$, $\text{Mg}(\text{HCOO})_2$,
563 $\text{Ca}(\text{CH}_3\text{COO})_2$ and $\text{Mg}(\text{CH}_3\text{COO})_2$ aerosols, measured in our work using H-TDMA. To the best
564 of our knowledge, this is the first time that GF of these four types of aerosols have been reported.
565 For $\text{Mg}(\text{HCOO})_2$, aerosol particles showed gradual while small growth for RH up to 30%, and
566 further increase in RH led to significant growth; the average GF of $\text{Mg}(\text{HCOO})_2$ aerosol at 90%
567 RH was determined to be 1.69 ± 0.03 , similar to those for $\text{Mg}(\text{NO}_3)_2$ (1.67 ± 0.03) and MgCl_2

568 (1.71±0.03) at the same RH. For RH up to 85%, Ca(HCOO)₂ aerosol particles exhibited gradual
 569 and small growth; when RH was increased to 90%, abrupt and large growth was observed, with
 570 GF being 1.54±0.02, significantly smaller than that for Mg(HCOO)₂ aerosol at the same RH. This
 571 is distinctively different from what was observed in VSA experiments, in which the mass of
 572 Ca(HCOO)₂ and Mg(HCOO)₂·2H₂O powdered samples was only increased by <5% when RH was
 573 increased from 0 to 95%. This difference may be explained by the different states of samples used
 574 in these two types of experiments (i. e. crystalline samples in VSA experiments, while likely
 575 amorphous aerosol particles in H-TDMA measurements), leading to different hygroscopic
 576 behaviors.



577
 578 **Figure 6.** Hygroscopic growth factors (GF) of aerosol particles as a function of RH measured
 579 using H-TDMA. (a): Ca(HCOO)₂ and Mg(HCOO)₂; (b) Ca(CH₃COO)₂ and Mg(CH₃COO)₂.

580
 581 As shown in Figure 6b, gradual and small growth was also observed for Ca(CH₃COO)₂
 582 and Mg(CH₃COO)₂ aerosols at low RH. Fast increase in GF started at about 80% RH for

583 $\text{Ca}(\text{CH}_3\text{COO})_2$ aerosol, and the GF was determined to be 1.26 ± 0.04 at 90% RH. As discussed in
584 Section 3.2.1, in VSA experiments no significant increase in sample mass was observed for
585 $\text{Ca}(\text{CH}_3\text{COO})_2\cdot\text{H}_2\text{O}$ when RH was increased from 0 to 90%, being different from H-TDMA results.
586 This difference may again be explained (at least partly) by different states of particles used in these
587 two types of experiments, as mentioned above. Careful inspection of Figure 6b and Table 6 reveals
588 that a small decrease in GF from 1.03 ± 0.01 to 1.00 ± 0.01 for $\text{Ca}(\text{CH}_3\text{COO})_2$ aerosol when RH was
589 increased from 50 to 70%. The decrease in GF may be caused by restructuring of particles or
590 change in particle morphology (Vlasenko et al., 2005; Koehler et al., 2009); in addition, the small
591 change in GF (~ 0.03) may not be significant when compared to the uncertainties in our H-TDMA
592 measurements.

593 When RH increased from 0 to 70%, small and gradual growth occurred for $\text{Mg}(\text{CH}_3\text{COO})_2$
594 aerosol particles, indicating that these particles may contain some amount of amorphous materials.
595 It was also found in previous work (Li et al., 2008a; Li et al., 2008b) that $\text{Mg}(\text{NO}_3)_2$ particles
596 generated by drying aqueous droplets were amorphous. Figure 6b reveals that further increase in
597 RH led to large increase in growth factors, and this is largely consistent with the occurrence of
598 deliquescence at $\sim 71.5\%$ RH at 25°C for $\text{Mg}(\text{CH}_3\text{COO})_2\cdot 4\text{H}_2\text{O}$, as mentioned in Section 3.2.1. At
599 90% RH, GF of $\text{Mg}(\text{CH}_3\text{COO})_2$ aerosol was determined to be 1.53 ± 0.01 , much larger than that for
600 $\text{Ca}(\text{CH}_3\text{COO})_2$ (1.26 ± 0.04).

601 At 90% RH, for the four Ca-containing salts considered in our study, nitrate and chloride
602 aerosols have very similar GF (1.79 ± 0.03 versus 1.71 ± 0.03), which are large than that of formate
603 (1.54 ± 0.02), and acetate has the smallest GF (1.26 ± 0.04). For comparison, the variation in GF at
604 90% RH was found to be considerably smaller (from ~ 1.53 to ~ 1.71) for the four Mg-containing
605 salts studied herein.

606

607 **Table 7.** Hygroscopic growth factors of $\text{Ca}(\text{HCOO})_2$, $\text{Ca}(\text{CH}_3\text{COO})_2$, $\text{Mg}(\text{HCOO})_2$ and
 608 $\text{Mg}(\text{CH}_3\text{COO})_2$ aerosol particles measured using H-TDMA. The absolute uncertainties in RH were
 609 estimated to be within $\pm 2\%$. All the errors given in this work are standard deviations.

RH (%)	$\text{Ca}(\text{HCOO})_2$	$\text{Ca}(\text{CH}_3\text{COO})_2$	$\text{Mg}(\text{HCOO})_2$	$\text{Mg}(\text{CH}_3\text{COO})_2$
5	1.00 \pm 0.01	1.00 \pm 0.01	1.00 \pm 0.01	1.00 \pm 0.01
10	1.01 \pm 0.01	1.01 \pm 0.01	1.02 \pm 0.01	1.01 \pm 0.01
20	1.01 \pm 0.01	1.01 \pm 0.02	1.02 \pm 0.01	1.01 \pm 0.01
30	1.01 \pm 0.01	1.01 \pm 0.01	1.02 \pm 0.01	1.02 \pm 0.01
40	1.01 \pm 0.01	1.02 \pm 0.01	1.04 \pm 0.01	1.02 \pm 0.01
50	1.02 \pm 0.01	1.03 \pm 0.01	1.11 \pm 0.01	1.04 \pm 0.01
60	1.02 \pm 0.01	1.01 \pm 0.01	1.18 \pm 0.01	1.04 \pm 0.01
70	1.03 \pm 0.01	1.00 \pm 0.01	1.27 \pm 0.01	1.10 \pm 0.02
75	1.04 \pm 0.01	1.02 \pm 0.02	1.33 \pm 0.01	1.16 \pm 0.02
80	1.04 \pm 0.01	1.07 \pm 0.01	1.41 \pm 0.01	1.25 \pm 0.01
85	1.01 \pm 0.01	1.13 \pm 0.01	1.52 \pm 0.02	1.37 \pm 0.01
90	1.54 \pm 0.02	1.26 \pm 0.04	1.69 \pm 0.03	1.53 \pm 0.01

610

611 According to Eq. (4), GF measured at 90% RH can be used to calculate κ_{gf} , which were
 612 determined to be 0.28-0.31 for $\text{Ca}(\text{HCOO})_2$, 0.09-0.13 for $\text{Ca}(\text{CH}_3\text{COO})_2$, 0.40-0.45 for
 613 $\text{Mg}(\text{HCOO})_2$, and 0.28-0.29 for $\text{Mg}(\text{CH}_3\text{COO})_2$. A previous study (Tang et al., 2015) investigated
 614 the CCN activities of $\text{Ca}(\text{HCOO})_2$ and $\text{Ca}(\text{CH}_3\text{COO})_2$ aerosols and reported their single
 615 hygroscopicity parameters (κ_{ccn}), while the CCN activities of $\text{Mg}(\text{HCOO})_2$ and $\text{Mg}(\text{CH}_3\text{COO})_2$
 616 have not been explored yet. As summarized in Table 5, κ_{ccn} was reported to be 0.47-0.52 for
 617 $\text{Ca}(\text{HCOO})_2$ (Tang et al., 2015), significantly larger than κ_{gf} (0.28-0.31) determined in our work;
 618 for $\text{Ca}(\text{CH}_3\text{COO})_2$, Tang et al. (2015) reported κ_{ccn} to be in the range of 0.37-0.47, again much
 619 larger than κ_{gf} (0.09-0.13) derived from the present work.

620 As discussed in Section 3.1.4, for $\text{Ca}(\text{NO}_3)_2$ and CaCl_2 aerosols, κ_{gf} derived from H-TDMA
621 experiments in the present work show fairly good agreement with κ_{ccn} derived from CCN activities
622 measured in previous studies (Tang et al., 2015; Sullivan et al., 2009); in contrast, for $\text{Ca}(\text{HCOO})_2$
623 and $\text{Ca}(\text{CH}_3\text{COO})_2$ aerosols, κ_{gf} derived from our H-TDMA experiments are significantly smaller
624 than κ_{ccn} reported by the previous study (Tang et al., 2015). This can be largely caused by the
625 difference in water solubilities of $\text{Ca}(\text{NO}_3)_2$, CaCl_2 , $\text{Ca}(\text{HCOO})_2$ and $\text{Ca}(\text{CH}_3\text{COO})_2$.
626 $\text{Ca}(\text{NO}_3)_2 \cdot 4\text{H}_2\text{O}$ and $\text{CaCl}_2 \cdot 6\text{H}_2\text{O}$, with solubilities being 1983 and 1597 g per kg water at 25 °C
627 (Kelly and Wexler, 2005), can be considered to be highly soluble; for comparison, the solubilities
628 were reported to be 166 g per kg water for $\text{Ca}(\text{HCOO})_2$ at 25 °C and 347 g per kg water for
629 $\text{Ca}(\text{CH}_3\text{COO})_2 \cdot 2\text{H}_2\text{O}$ at 20 °C (Dean, 1973). Due to their limited water solubilities, $\text{Ca}(\text{HCOO})_2$
630 and $\text{Ca}(\text{CH}_3\text{COO})_2$ aerosol particles may not be fully dissolved at 90% RH in the H-TDMA
631 experiments but would be dissolved to a larger extent (if not completely) for RH >100% in CCN
632 activity measurements (Kreidenweis and Asa-Awuku, 2014; Petters and Kreidenweis, 2008).
633 Therefore, for $\text{Ca}(\text{HCOO})_2$ and $\text{Ca}(\text{CH}_3\text{COO})_2$ aerosols, κ_{gf} derived from H-TDMA measurements
634 would be smaller than κ_{ccn} derived from CCN activity measurements. In fact, the observation that
635 κ_{gf} appeared to be significantly smaller than κ_{ccn} , largely caused by limited water solubilities of
636 compounds under investigation, has been well documented in the literature for laboratory-
637 generated and ambient aerosol particles (Massoli et al., 2010; Prenni et al., 2007; Wex et al.,
638 2009; Good et al., 2010; Chang et al., 2007).

639 **3.3 Discussion**

640 **3.3.1 Comparison between H-TDMA and VSA measurements**

641 In this work two complementary techniques were employed to investigate the hygroscopic
642 properties of Ca- and Mg-containing compounds. The mass change of bulk samples was measured

643 as a function of RH using VSA, and the change in aerosol diameter with RH was determined using
644 H-TDMA. Two major questions can be asked regarding the results obtained using the two different
645 techniques: 1) How can the two types of results be reconciled? 2) What is the atmospheric
646 relevance of each type of results? Below we use $\text{Ca}(\text{NO}_3)_2$ at room temperature as an example for
647 discussion, and similar conclusions can be drawn for the other seven compounds.

648 As presented in Section 3.1, at 25 °C the deliquescence of $\text{Ca}(\text{NO}_3)_2 \cdot 4\text{H}_2\text{O}$ took place at
649 52-53% RH. In contrast, dry $\text{Ca}(\text{NO}_3)_2$ aerosol particles generated by atomizing aqueous solutions
650 were likely to be amorphous (Gibson et al., 2006; Tang and Fung, 1997; Al-Abadleh et al., 2003);
651 as a result, they exhibited continuous hygroscopic growth with increasing RH with no distinct
652 solid-liquid phase transitions observed. When RH exceed the DRH of $\text{Ca}(\text{NO}_3)_2 \cdot 4\text{H}_2\text{O}$, both
653 $\text{Ca}(\text{NO}_3)_2 \cdot 4\text{H}_2\text{O}$ bulk samples and $\text{Ca}(\text{NO}_3)_2$ aerosol particles are expected to deliquesce to form
654 aqueous solutions. To directly link the mass change (measured using VSA) with diameter change
655 (measured using H-TDMA), solution densities, which also vary with RH, are needed. Two
656 important outputs of common aerosol thermodynamic models, such as E-AIM (Clegg et al., 1998)
657 and ISORROPIA II (Fountoukis and Nenes, 2007) are volumes and water-to-solute ratios as a
658 function of RH (above DRH) for aqueous solutions. Water-to-solute ratios and particle diameters
659 were both measured in our work at different RH, and our experimental data, when compared with
660 theoretical calculations, can be used to validate these thermodynamic models.

661 When RH are lower than the DRH of $\text{Ca}(\text{NO}_3)_2 \cdot 4\text{H}_2\text{O}$, aerosol particles used in our H-
662 TDMA experiments, instead of bulk samples used in the VSA measurements, are of direct
663 atmospheric relevance, and hence the H-TDMA results should be used in atmospheric implications.
664 There are still some open questions regarding $\text{Ca}(\text{NO}_3)_2$ aerosol particles (as well as other types of
665 particles investigated in this work) for RH below DRH of $\text{Ca}(\text{NO}_3)_2 \cdot 4\text{H}_2\text{O}$. What is the phase state

666 of aerosol particles at different RH? Are they crystalline solid, amorphous solid (glassy), or
667 supersaturated solutions? In this aspect, measurements of particle phase state of $\text{Ca}(\text{NO}_3)_2$ and
668 other aerosols considered in our work, using the apparatus described previously (Li et al., 2017),
669 can shed some light. Furthermore, how do water-to-solute ratios change with RH for $\text{Ca}(\text{NO}_3)_2$
670 aerosol particles when RH is below the DRH of $\text{Ca}(\text{NO}_3)_2 \cdot 4\text{H}_2\text{O}$? This can be answered by
671 determining particle mass as a function of RH for aerosol particles, and techniques are now
672 available for this task (Vlasenko et al., 2017).

673 **3.3.2 Atmospheric implications**

674 Hygroscopicity of carbonate minerals, such as calcite and dolomite, is initially very low
675 and can be largely enhanced due to formation of more hygroscopic materials via heterogeneous
676 reactions during transport (Tang et al., 2016a). Our present work investigated the hygroscopic
677 properties of eight Ca- or Mg-containing compounds which are aging products formed via
678 heterogeneous reactions of carbonate minerals, and revealed that the hygroscopicity of these
679 products is significantly higher than original carbonate minerals. In addition, hygroscopicity was
680 found to differ for different aging products, suggesting that heterogeneous reactions with different
681 trace gases may have distinctive effects on the hygroscopicity of carbonate minerals. For example,
682 the hygroscopicity of $\text{Ca}(\text{NO}_3)_2$ and CaCl_2 , formed through heterogeneous reactions with nitrogen
683 oxides and HCl, is much higher than that for $\text{Ca}(\text{HCOO})_2$ and $\text{Ca}(\text{CH}_3\text{COO})_2$, formed via
684 heterogeneous reactions with formic and acetic acids. Our work also observed that significant
685 hygroscopic growth of aerosol particles, such as $\text{Ca}(\text{NO}_3)_2$ and CaCl_2 , occurred at RH as low as
686 10%. This implies that aged carbonate particles can take up significant amount of water even under
687 very low RH, leading to changes in their diameters and morphology and thus impacting their
688 optical properties and direct radiative forcing effects (Pan et al., 2015; Pan et al., 2018).

689 Large amounts of saline mineral dust are emitted into the atmosphere from dry lake beds
690 (Prospero et al., 2002), but these particles are usually assumed to be nonhygroscopic. Gaston et al.
691 (2017) found that saline mineral dust particles from different sources exhibit very different CCN
692 activities, and the measured κ_{ccn} varied from <0.01 to >0.8 , depending on the abundance of soluble
693 components (e.g., chlorides and sulfates) contained in these particles. Saline mineral dust particles
694 are very likely to have different hygroscopic properties under subsaturation. To understand the
695 hygroscopic growth of saline mineral dust particles, knowledge in hygroscopic growth as well as
696 the abundance of soluble components they contain is needed. Since CaCl_2 and MgCl_2 have been
697 identified as important components in saline mineral dust, their hygroscopicity data measured in
698 our work will be useful for improving our knowledge in hygroscopic properties of saline mineral
699 dust.

700 It is conventionally assumed that the hygroscopicity of sea salt is very similar to that of
701 pure NaCl. However, a recent study (Zieger et al., 2017) suggested that the hygroscopic growth
702 factor of sea salt aerosol at 90% RH is 8-15% lower than NaCl aerosol, and this difference is
703 attributed to the presence of MgCl_2 and CaCl_2 hydrates in sea salt. Growth factors at 90% RH were
704 measured in our work to be ~ 1.7 for MgCl_2 and CaCl_2 aerosols, significant lower than for NaCl
705 (2.29-2.46) (Zieger et al., 2017). Therefore, our work provides further experimental results to
706 support the conclusion drawn by Zieger et al., and would help better understand the hygroscopicity
707 of sea salt aerosol.

708 **4. Summary and Conclusion**

709 Ca- and Mg-containing salts, including nitrates, chlorides, formates and acetates, are
710 important components for mineral dust and sea salt aerosols; however, their hygroscopic properties
711 are not well understood yet. In this work, phase transition and hygroscopic growth of eight Ca- or

712 Mg-containing compounds were systematically examined using a vapor sorption analyzer and a
713 humidity-tandem differential mobility analyzer. DRH values decreased from $60.5\pm 1.0\%$ at $5\text{ }^{\circ}\text{C}$ to
714 $46.0\pm 1.0\%$ at $30\text{ }^{\circ}\text{C}$ for $\text{Ca}(\text{NO}_3)_2\cdot 4\text{H}_2\text{O}$ and from $57.5\pm 1.0\%$ at $5\text{ }^{\circ}\text{C}$ to $50.5\pm 1.0\%$ at $30\text{ }^{\circ}\text{C}$ for
715 $\text{Mg}(\text{NO}_3)_2\cdot 6\text{H}_2\text{O}$, both showing negative dependence on temperature, and the dependence of their
716 DRH on temperature can be approximated by the Clausius-Clapeyron equation. No significant
717 dependence of DRH (around 31-33%) on temperature ($5\text{-}30\text{ }^{\circ}\text{C}$) was observed for $\text{MgCl}_2\cdot 6\text{H}_2\text{O}$.
718 $\text{CaCl}_2\cdot 6\text{H}_2\text{O}$, found to deliquesce at $\sim 28.5\%$ RH at $25\text{ }^{\circ}\text{C}$, exhibited complex phase transition
719 processes in which $\text{CaCl}_2\cdot 2\text{H}_2\text{O}$, $\text{CaCl}_2\cdot 6\text{H}_2\text{O}$ and aqueous CaCl_2 solutions were involved.
720 Furthermore, DRH values were determined to be $90.5\pm 1.0\%$ for $\text{Ca}(\text{CH}_3\text{COO})_2\cdot \text{H}_2\text{O}$ and $71.5\pm 1.0\%$
721 for $\text{Mg}(\text{CH}_3\text{COO})_2\cdot 4\text{H}_2\text{O}$ at $25\text{ }^{\circ}\text{C}$; for comparison, the sample mass was only increased by $<5\%$
722 for $\text{Ca}(\text{HCOO})_2$ and $\text{Mg}(\text{HCOO})_2\cdot 2\text{H}_2\text{O}$ when RH was increased from 0 to 95%, suggesting that
723 the DRH of these two compounds were $>95\%$.

724 We have also measured the change of sample mass as a function of RH up to 90% to derive
725 the water-to-solute ratios (WSR) for deliquesced samples. WSR were determined at 25 and $5\text{ }^{\circ}\text{C}$
726 for deliquesced $\text{Ca}(\text{NO}_3)_2\cdot 4\text{H}_2\text{O}$, $\text{Mg}(\text{NO}_3)_2\cdot 6\text{H}_2\text{O}$ and $\text{MgCl}_2\cdot 6\text{H}_2\text{O}$ samples, and at $25\text{ }^{\circ}\text{C}$ for
727 deliquesced $\text{CaCl}_2\cdot 6\text{H}_2\text{O}$ and $\text{Mg}(\text{CH}_3\text{COO})_2\cdot 4\text{H}_2\text{O}$ samples. We found that compared to that at 0%
728 RH, large increases in sample mass only occurred when RH was increased from 90 to 95% for
729 $\text{Ca}(\text{CH}_3\text{COO})_2\cdot \text{H}_2\text{O}$, and the WSR value was determined to be 5.849 ± 0.064 at 95% RH. Besides,
730 deliquescence was not observed even when RH was increased to 95% for $\text{Ca}(\text{HCOO})_2$ and
731 $\text{Mg}(\text{HCOO})_2\cdot 2\text{H}_2\text{O}$, and the ratios of sample mass at 95% to that at 0% RH, were determined to
732 be for 1.043 ± 0.018 for $\text{Ca}(\text{HCOO})_2$ and 1.028 ± 0.008 for $\text{Mg}(\text{HCOO})_2\cdot 2\text{H}_2\text{O}$. Despite that these
733 compounds are important components for tropospheric aerosols, in general they have not been
734 included in widely used aerosol thermodynamic models, such as E-AIM (Clegg et al., 1998) and

735 ISORROPIA II (Fountoukis and Nenes, 2007). The systematical and comprehensive datasets
736 which we have obtained in this work are highly valuable and can be used to validate
737 thermodynamic models if they are extended to include these compounds.

738 In addition, hygroscopic growth of aerosol particles was measured at room temperature for
739 these eight compounds. Being different from solid samples for which the onset of deliquescence
740 was evident, aerosol particles were found to grow in a continuous manner since very low RH (as
741 low as 10%), implying that dry aerosol particles of these eight compounds generated from aqueous
742 droplets were amorphous. Hygroscopic growth factors of aerosol particles at 90% RH were
743 determined to be 1.79 ± 0.03 and 1.67 ± 0.03 for $\text{Ca}(\text{NO}_3)_2$ and $\text{Mg}(\text{NO}_3)_2$, 1.71 ± 0.03 for both CaCl_2
744 and MgCl_2 , 1.54 ± 0.02 and 1.69 ± 0.03 for $\text{Ca}(\text{HCOO})_2$ and $\text{Mg}(\text{HCOO})_2$, and 1.26 ± 0.04 and
745 1.53 ± 0.01 for $\text{Ca}(\text{HCOO})_2$ and $\text{Mg}(\text{HCOO})_2$. GF at 90% show significant variation (from ~ 1.26
746 to ~ 1.79) for the Ca-containing salts investigated here; among them nitrate and chloride have very
747 similar GF (1.79 ± 0.03 versus 1.71 ± 0.03), which are larger than that of formate (1.54 ± 0.02), while
748 acetate has the smallest GF (1.26 ± 0.04). Interestingly, for the four Mg-containing salts considered
749 in this work, the variation in GF at 90 % RH was found to be much smaller (from ~ 1.53 to ~ 1.71).

750 GF at 90% RH were used to derive the single hygroscopicity parameters (κ), which were
751 determined to be 0.49-0.56 and 0.38-0.43 for $\text{Ca}(\text{NO}_3)_2$ and $\text{Mg}(\text{NO}_3)_2$, 0.42-0.47 for both CaCl_2
752 and MgCl_2 , 0.28-0.31 and 0.40-0.45 for $\text{Ca}(\text{HCOO})_2$ and $\text{Mg}(\text{HCOO})_2$, and 0.09-0.13 and 0.28-
753 0.29 for $\text{Ca}(\text{HCOO})_2$ and $\text{Mg}(\text{HCOO})_2$ aerosols, respectively. $\text{Ca}(\text{NO}_3)_2$ and CaCl_2 are very soluble
754 in water, and thus their κ values derived from our H-TDMA experiments are consistent with those
755 reported by previous CCN activity measurements (Tang et al., 2015; Sullivan et al., 2009); on the
756 other hand, due to limited water solubilities, for $\text{Ca}(\text{HCOO})_2$ and $\text{Ca}(\text{CH}_3\text{COO})_2$, κ values derived
757 from our H-TDMA experiments are significantly smaller than those derived from CCN activities

758 in a previous study (Tang et al., 2015). Overall, the present work would significantly improve our
759 knowledge in the hygroscopic properties of Ca- and Mg-containing salts, and thereby help better
760 understand the physicochemical properties of mineral dust and sea salt aerosols.

761 **Author contribution**

762 Mingjin Tang designed the research; Liya Guo, Peng Chao, Taomou Zong, Qin hao Lin and
763 Guohua Zhang did the H-TDMA experiments and analyzed the results with the assistance and
764 supervision of Weigang Wang, Zhijun Wu, Maofa Ge, Min Hu and Xinhui Bi; Wenjun Gu and
765 Yujing Tang did the VSA experiments and analyzed the data with the supervision of Yong Jie Li,
766 Xinming Wang and Mingjin Tang; Yong Jie Li and Mingjin Tang wrote the manuscript with the
767 contribution from all the other co-authors.

768 **Acknowledgement**

769 Financial support provided by the National Natural Science Foundation of China
770 (91744204, 91644106 and 41675120), the Chinese Academy of Sciences international
771 collaborative project (132744KYSB20160036) and the special fund of State Key Joint Laboratory
772 of Environment Simulation and Pollution Control (17K02ESPCP) is acknowledged. Mingjin Tang
773 also would like to thank the CAS Pioneer Hundred Talents program for providing a starting grant.
774 Yujing Tang contributed to this work as an undergraduate intern at Guangzhou Institute of
775 Geochemistry.

776 **References**

- 777 Adams, J. R., and Merz, A. R.: Hygroscopicity of Fertilizer Materials and Mixtures, *Ind. Eng. Chem.*, 21, 305-307,
778 1929.
779 Al-Abadleh, H. A., and Grassian, V. H.: Phase transitions in magnesium nitrate thin films: A transmission FT-IR
780 study of the deliquescence and efflorescence of nitric acid reacted magnesium oxide interfaces, *J. Phys. Chem. B*,
781 107, 10829-10839, 2003.
782 Al-Abadleh, H. A., Krueger, B. J., Ross, J. L., and Grassian, V. H.: Phase transitions in calcium nitrate thin films,
783 *Chem. Commun.*, 2796-2797, 2003.

784 Apelblat, A.: The vapor pressures of water over saturated solutions of barium chloride, magnesium nitrate, calcium
785 nitrate, potassium carbonate, and zinc sulfate at temperatures from 283 K to 323 K, *J. Chem. Thermodyn.*, 24, 619-
786 626, 1992.

787 Biggs, A. I., Parton, H. N., and Robinson, R. A.: The Constitution of the Lead Halides in Aqueous Solution, *J. Am.*
788 *Chem. Soc.*, 77, 5844-5848, 1955.

789 Chang, R. Y. W., Liu, P. S. K., Leaitch, W. R., and Abbatt, J. P. D.: Comparison between measured and predicted
790 CCN concentrations at Egbert, Ontario: Focus on the organic aerosol fraction at a semi-rural site, *Atmos. Environ.*,
791 41, 8172-8182, 2007.

792 Chen, S. Y., Huang, J. P., Kang, L. T., Wang, H., Ma, X. J., He, Y. L., Yuan, T. G., Yang, B., Huang, Z. W., and
793 Zhang, G. L.: Emission, transport, and radiative effects of mineral dust from the Taklimakan and Gobi deserts:
794 comparison of measurements and model results, *Atmos. Chem. Phys.*, 17, 2401-2421, 2017.

795 Clegg, S. L., Brimblecombe, P., and Wexler, A. S.: Thermodynamic Model of the System $H^+-NH_4^+-Na^+-SO_4^{2-}$
796 $-NO_3^- -Cl^- -H_2O$ at 298.15 K, *J. Phys. Chem. A.*, 102, 2155-2171, 1998.

797 Creamean, J. M., Suski, K. J., Rosenfeld, D., Cazorla, A., DeMott, P. J., Sullivan, R. C., White, A. B., Ralph, F. M.,
798 Minnis, P., Comstock, J. M., Tomlinson, J. M., and Prather, K. A.: Dust and Biological Aerosols from the Sahara
799 and Asia Influence Precipitation in the Western U.S, *Science*, 339, 1572-1578, 2013.

800 Crowley, J. N., Ammann, M., Cox, R. A., Hynes, R. G., Jenkin, M. E., Mellouki, A., Rossi, M. J., Troe, J., and
801 Wallington, T. J.: Evaluated Kinetic and Photochemical Data for Atmospheric Chemistry: Volume V -
802 Heterogeneous Reactions on Solid Substrates, *Atmos. Chem. Phys.*, 10, 9059-9223, 2010.

803 Cziczco, D. J., and Abbatt, J. P. D.: Infrared observations of the response of NaCl, MgCl₂, NH₄HSO₄, and NH₄NO₃
804 aerosols to changes in relative humidity from 298 to 238 K, *J. Phys. Chem. A*, 104, 2038-2047, 2000.

805 Cziczco, D. J., Froyd, K. D., Hoose, C., Jensen, E. J., Diao, M., Zondlo, M. A., Smith, J. B., Twohy, C. H., and
806 Murphy, D. M.: Clarifying the Dominant Sources and Mechanisms of Cirrus Cloud Formation, *Science*, 340, 1320-
807 1324, 2013.

808 Dean, J. A.: *Lange's Handbook on Chemistry (Eleventh Edition)*, McGraw-Hill, Inc., New York, 1973.

809 El Guendouzi, M., and Marouani, M.: Water activities and osmotic and activity coefficients of aqueous solutions of
810 nitrates at 25 degrees C by the hygrometric method, *J. Solution Chem.*, 32, 535-546, 2003.

811 Formenti, P., Rajot, J. L., Desboeufs, K., Saïd, F., Grand, N., Chevaillier, S., and Schmechtig, C.: Airborne
812 observations of mineral dust over western Africa in the summer Monsoon season: spatial and vertical variability of
813 physico-chemical and optical properties, *Atmos. Chem. Phys.*, 11, 6387-6410, 2011.

814 Formenti, P., Caquineau, S., Desboeufs, K., Klaver, A., Chevaillier, S., Journet, E., and Rajot, J. L.: Mapping the
815 physico-chemical properties of mineral dust in western Africa: mineralogical composition, *Atmos. Chem. Phys.*, 14,
816 10663-10686, 2014.

817 Fountoukis, C., and Nenes, A.: ISORROPIA II: a computationally efficient thermodynamic equilibrium model for
818 $K^+-Ca^{2+}-Mg^{2+}-NH_4^+-Na^+-SO_4^{2-}-NO_3^- -Cl^- -H_2O$ aerosols, *Atmos. Chem. Phys.*, 7, 4639-4659, 2007.

819 Gaston, C. J., Pratt, K. A., Suski, K. J., May, N. W., Gill, T. E., and Prather, K. A.: Laboratory Studies of the Cloud
820 Droplet Activation Properties and Corresponding Chemistry of Saline Playa Dust, *Environ. Sci. Technol.*, 51, 1348-
821 1356, 2017.

822 Gibson, E. R., Hudson, P. K., and Grassian, V. H.: Physicochemical properties of nitrate aerosols: Implications for
823 the atmosphere, *J. Phys. Chem. A*, 110, 11785-11799, 2006.

824 Ginoux, P., Prospero, J. M., Gill, T. E., Hsu, N. C., and Zhao, M.: Global-scale Attribution of Anthropogenic and
825 Natural Dust Sources and Their Emission Rates Based on MODIS Deep Blue Aerosol Products, *Rev. Geophys.*, 50,
826 RG3005, doi: 3010.1029/2012RG000388, 2012.

827 Good, N., Topping, D. O., Duplissy, J., Gysel, M., Meyer, N. K., Metzger, A., Turner, S. F., Baltensperger, U.,
828 Ristovski, Z., Weingartner, E., Coe, H., and McFiggans, G.: Widening the gap between measurement and modelling
829 of secondary organic aerosol properties?, *Atmos. Chem. Phys.*, 10, 2577-2593, 2010.

830 Goodman, A. L., Underwood, G. M., and Grassian, V. H.: A Laboratory Study of the Heterogeneous Reaction of
831 Nitric Acid on Calcium Carbonate Particles, *J. Geophys. Res.-Atmos.*, 105, 29053-29064, 2000.

832 Gough, R. V., Chevrier, V. F., and Tolbert, M. A.: Formation of liquid water at low temperatures via the
833 deliquescence of calcium chloride: Implications for Antarctica and Mars, *Planet. Space Sci.*, 131, 79-87, 2016.

834 Gu, W. J., Li, Y. J., Tang, M. J., Jia, X. H., Ding, X., Bi, X. H., and Wang, X. M.: Water uptake and hygroscopicity
835 of perchlorates and implications for the existence of liquid water in some hyperarid environments, *RSC Adv.*, 7,
836 46866-46873, 2017a.

837 Gu, W. J., Li, Y. J., Zhu, J. X., Jia, X. H., Lin, Q. H., Zhang, G. H., Ding, X., Song, W., Bi, X. H., Wang, X. M., and
838 Tang, M. J.: Investigation of water adsorption and hygroscopicity of atmospherically relevant particles using
839 a commercial vapor sorption analyzer, *Atmos. Meas. Tech.*, 10, 3821-3832, 2017b.

840 Gupta, D., Eom, H. J., Cho, H. R., and Ro, C. U.: Hygroscopic behavior of NaCl-MgCl₂ mixture particles as nascent
841 sea-spray aerosol surrogates and observation of efflorescence during humidification, *Atmos. Chem. Phys.*, 15,
842 11273-11290, 2015.

843 Gysel, M., McFiggans, G. B., and Coe, H.: Inversion of tandem differential mobility analyser (TDMA)
844 measurements, *J. Aerosol. Sci.*, 40, 134-151, 2009.

845 Ha, Z., and Chan, C. K.: The Water Activities of MgCl₂, Mg(NO₃)₂, MgSO₄, and Their Mixtures, *Aerosol Sci.*
846 *Technol.*, 31, 154-169, 1999.

847 Hatch, C. D., Gough, R. V., and Tolbert, M. A.: Heterogeneous Uptake of the C1 to C4 Organic Acids on a Swelling
848 Clay Mineral, *Atmos. Chem. Phys.*, 7, 4445-4458, 2007.

849 Hoose, C., and Moehler, O.: Heterogeneous ice nucleation on atmospheric aerosols: a review of results from
850 laboratory experiments, *Atmos. Chem. Phys.*, 12, 9817-9854, 2012.

851 Jeong, G. Y., and Achterberg, E. P.: Chemistry and mineralogy of clay minerals in Asian and Saharan dusts and the
852 implications for iron supply to the oceans, *Atmos. Chem. Phys.*, 14, 12415-12428, 2014.

853 Jia, X. H., Gu, W. J., Li, Y. J., Cheng, P., Tang, Y. J., Guo, L. Y., Wang, X. M., and Tang, M. J.: Phase transitions
854 and hygroscopic growth of Mg(ClO₄)₂, NaClO₄, and NaClO₄·H₂O: implications for the stability of aqueous water
855 in hyperarid environments on Mars and on Earth, *ACS Earth Space Chem.*, 2, 159-167, 2018.

856 Jickells, T. D., An, Z. S., Andersen, K. K., Baker, A. R., Bergametti, G., Brooks, N., Cao, J. J., Boyd, P. W., Duce,
857 R. A., Hunter, K. A., Kawahata, H., Kubilay, N., laRoche, J., Liss, P. S., Mahowald, N., Prospero, J. M., Ridgwell,
858 A. J., Tegen, I., and Torres, R.: Global Iron Connections between Desert Dust, Ocean Biogeochemistry, and
859 Climate, *Science*, 308, 67-71, 2005.

860 Jing, B., Tong, S. R., Liu, Q. F., Li, K., Wang, W. G., Zhang, Y. H., and Ge, M. F.: Hygroscopic behavior of
861 multicomponent organic aerosols and their internal mixtures with ammonium sulfate, *Atmos. Chem. Phys.*, 16,
862 4101-4118, 2016.

863 Jing, B., Wang, Z., Tan, F., Guo, Y. C., Tong, S. R., Wang, W. G., Zhang, Y. H., and Ge, M. F.: Hygroscopic
864 behavior of atmospheric aerosols containing nitrate salts and water-soluble organic acids, *Atmos. Chem. Phys.*, 18,
865 5115-5127, 2018.

866 Journet, E., Balkanski, Y., and Harrison, S. P.: A New Data Set of Soil Mineralogy for Dust-cycle Modeling, *Atmos.*
867 *Chem. Phys.*, 14, 3801-3816, 2014.

868 Kelly, J. T., and Wexler, A. S.: Thermodynamics of carbonates and hydrates related to heterogeneous reactions
869 involving mineral aerosol, *J. Geophys. Res.-Atmos.*, 110, D11201, doi: 11210.11029/12004jd005583, 2005.

870 Kelly, J. T., Chuang, C. C., and Wexler, A. S.: Influence of dust composition on cloud droplet formation, *Atmos.*
871 *Environ.*, 41, 2904-2916, 2007.

872 Khare, P., Kumar, N., Kumari, K. M., and Srivastava, S. S.: Atmospheric formic and acetic acids: An overview,
873 *Rev. Geophys.*, 37, 227-248, 1999.

874 Koehler, K. A., Kreidenweis, S. M., DeMott, P. J., Petters, M. D., Prenni, A. J., and Carrico, C. M.: Hygroscopicity
875 and cloud droplet activation of mineral dust aerosol, *Geophys. Res. Lett.*, 36, L08805, doi:
876 08810.01029/02009gl037348, 2009.

877 Kreidenweis, S. M., and Asa-Awuku, A.: 5.13 - Aerosol Hygroscopicity: Particle Water Content and Its Role in
878 Atmospheric Processes, in: *Treatise on Geochemistry (Second Edition)*, edited by: Turekian, K. K., Elsevier,
879 Oxford, 331-361, 2014.

880 Krueger, B. J., Grassian, V. H., Laskin, A., and Cowin, J. P.: The Transformation of Solid Atmospheric Particles
881 into Liquid Droplets through Heterogeneous Chemistry: Laboratory Insights into the Processing of Calcium
882 Containing Mineral Dust Aerosol in the Troposphere, *Geophys. Res. Lett.*, 30, 1148, doi: 1110.1029/2002gl016563,
883 2003.

884 Laskin, A., Iedema, M. J., Ichkovich, A., Graber, E. R., Taraniuk, I., and Rudich, Y.: Direct Observation of
885 Completely Processed Calcium Carbonate Dust Particles, *Faraday Discuss.*, 130, 453-468, 2005.

886 Lei, T., Zuend, A., Wang, W. G., Zhang, Y. H., and Ge, M. F.: Hygroscopicity of organic compounds from biomass
887 burning and their influence on the water uptake of mixed organic ammonium sulfate aerosols, *Atmos. Chem. Phys.*,
888 14, 11165-11183, 2014.

889 Li, H. J., Zhu, T., Zhao, D. F., Zhang, Z. F., and Chen, Z. M.: Kinetics and mechanisms of heterogeneous reaction of
890 NO₂ on CaCO₃ surfaces under dry and wet conditions, *Atmos. Chem. Phys.*, 10, 463-474, 2010.

891 Li, W. J., and Shao, L. Y.: Observation of Nitrate Coatings on Atmospheric Mineral Dust Particles, *Atmos. Chem.*
892 *Phys.*, 9, 1863-1871, 2009.

893 Li, X.-H., Zhao, L.-J., Dong, J.-L., Xiao, H.-S., and Zhang, Y.-H.: Confocal Raman Studies of Mg(NO₃)₂ Aerosol
894 Particles Deposited on a Quartz Substrate: Supersaturated Structures and Complicated Phase Transitions, *J. Phys.*
895 *Chem. B.*, 112, 5032-5038, 2008a.

896 Li, X., Dong, J., Xiao, H., Lu, P., Hu, Y., and Zhang, Y.: FTIR-ATR in situ observation on the efflorescence and
897 deliquescence processes of $Mg(NO_3)_2$ aerosols, *Sci. China-Chem.*, 51, 128-137, 2008b.

898 Li, Y. J., Liu, P. F., Bergoend, C., Bateman, A. P., and Martin, S. T.: Rebounding hygroscopic inorganic aerosol
899 particles: Liquids, gels, and hydrates, *Aerosol Sci. Technol.*, 51, 388-396, 2017.

900 Liu, Y., Gibson, E. R., Cain, J. P., Wang, H., Grassian, V. H., and Laskin, A.: Kinetics of heterogeneous reaction of
901 $CaCO_3$ particles with gaseous HNO_3 over a wide range of humidity, *J. Phys. Chem. A*, 112, 1561-1571, 2008a.

902 Liu, Y. J., Zhu, T., Zhao, D. F., and Zhang, Z. F.: Investigation of the hygroscopic properties of $Ca(NO_3)_2$ and
903 internally mixed $Ca(NO_3)_2/CaCO_3$ particles by micro-Raman spectrometry, *Atmos. Chem. Phys.*, 8, 7205-7215,
904 2008b.

905 Ma, Q. X., Liu, Y. C., Liu, C., and He, H.: Heterogeneous Reaction of Acetic Acid on MgO , $\alpha-Al_2O_3$, and $CaCO_3$
906 and the Effect on the Hygroscopic Behavior of These Particles, *Phys. Chem. Chem. Phys.*, 14, 8403-8409, 2012.

907 Mahowald, N., Ward, D. S., Kloster, S., Flanner, M. G., Heald, C. L., Heavens, N. G., Hess, P. G., Lamarque, J.-F.,
908 and Chuang, P. Y.: Aerosol Impacts on Climate and Biogeochemistry, *Annu. Rev. Environ. Resour.*, 36, 45-74,
909 2011.

910 Mahowald, N. M., Engelstaedter, S., Luo, C., Sealy, A., Artaxo, P., Benitez-Nelson, C., Bonnet, S., Chen, Y.,
911 Chuang, P. Y., Cohen, D. D., Dulac, F., Herut, B., Johansen, A. M., Kubilay, N., Losno, R., Maenhaut, W., Paytan,
912 A., Prospero, J. M., Shank, L. M., and Siefert, R. L.: Atmospheric Iron Deposition: Global Distribution, Variability,
913 and Human Perturbations, *Ann. Rev. Mar. Sci.*, 1, 245-278, 2009.

914 Massoli, P., Lambe, A. T., Ahern, A. T., Williams, L. R., Ehn, M., Mikkila, J., Canagaratna, M. R., Brune, W. H.,
915 Onasch, T. B., Jayne, J. T., Petaja, T., Kulmala, M., Laaksonen, A., Kolb, C. E., Davidovits, P., and Worsnop, D. R.:
916 Relationship between aerosol oxidation level and hygroscopic properties of laboratory generated secondary organic
917 aerosol (SOA) particles, *Geophys. Res. Lett.*, 37, L24801, DOI: 24810.21029/22010GL045258, 2010.

918 Nickovic, S., Vukovic, A., Vujadinovic, M., Djurdjevic, V., and Pejanovic, G.: Technical Note: High-resolution
919 mineralogical database of dust-productive soils for atmospheric dust modeling, *Atmos. Chem. Phys.*, 12, 845-855,
920 2012.

921 Pan, X., Uno, I., Hara, Y., Kuribayashi, M., Kobayashi, H., Sugimoto, N., Yamamoto, S., Shimohara, T., and Wang,
922 Z.: Observation of the simultaneous transport of Asian mineral dust aerosols with anthropogenic pollutants using a
923 POPC during a long-lasting dust event in late spring 2014, *Geophys. Res. Lett.*, 42, 1593-1598, 2015.

924 Pan, X., Uno, I., Wang, Z., Nishizawa, T., Sugimoto, N., Yamamoto, S., Kobayashi, H., Sun, Y., Fu, P., Tang, X.,
925 and Wang, Z.: Real-time observational evidence of changing Asian dust morphology with the mixing of heavy
926 anthropogenic pollution, *Sci. Rep.*, 7, 335, doi: 310.1038/s41598-41017-00444-w, 2017.

927 Pan, X., Ge, B., Wang, Z., Tian, Y., Liu, H., Wei, L., Yue, S., Uno, I., Kobayashi, H., Nishizawa, T., Shimizu, A.,
928 Fu, P., and Wang, Z.: Synergistic effect of water-soluble species and relative humidity on morphological changes of
929 aerosol particles in Beijing mega-city during severe pollution episodes, *Atmos. Chem. Phys. Discuss.*, 2018, 1-24,
930 10.5194/acp-2018-623, 2018.

931 Pang, S. F., Wu, C. Q., Zhang, Q. N., and Zhang, Y. H.: The structural evolution of magnesium acetate complex in
932 aerosols by FTIR-ATR spectra, *J. Mol. Struct.*, 1087, 46-50, 2015.

933 Park, K., Kim, J. S., and Miller, A. L.: A study on effects of size and structure on hygroscopicity of nanoparticles
934 using a tandem differential mobility analyzer and TEM, *J. Nanopart. Res.*, 11, 175-183, 2009.

935 Peng, C., Jing, B., Guo, Y. C., Zhang, Y. H., and Ge, M. F.: Hygroscopic Behavior of Multicomponent Aerosols
936 Involving NaCl and Dicarboxylic Acids, *J. Phys. Chem. A*, 120, 1029-1038, 2016.

937 Petters, M. D., and Kreidenweis, S. M.: A single parameter representation of hygroscopic growth and cloud
938 condensation nucleus activity, *Atmos. Chem. Phys.*, 7, 1961-1971, 2007.

939 Petters, M. D., and Kreidenweis, S. M.: A single parameter representation of hygroscopic growth and cloud
940 condensation nucleus activity-Part 2: Including solubility, *Atmos. Chem. Phys.*, 8, 6273-6279, 2008.

941 Petters, M. D., Wex, H., Carrico, C. M., Hallbauer, E., Massling, A., McMeeking, G. R., Poulain, L., Wu, Z.,
942 Kreidenweis, S. M., and Stratmann, F.: Towards closing the gap between hygroscopic growth and activation for
943 secondary organic aerosol - Part 2: Theoretical approaches, *Atmos. Chem. Phys.*, 9, 3999-4009, 2009.

944 Prenni, A. J., Petters, M. D., Kreidenweis, S. M., DeMott, P. J., and Ziemann, P. J.: Cloud droplet activation of
945 secondary organic aerosol, *J. Geophys. Res.-Atmos.*, 112, D10223, DOI: 10210.11029/12006JD007963, 2007.

946 Prince, A. P., Kleiber, P. D., Grassian, V. H., and Young, M. A.: Reactive Uptake of Acetic Acid on Calcite and
947 Nitric Acid Reacted Calcite Aerosol in an Environmental Reaction Chamber, *Phys. Chem. Chem. Phys.*, 10, 142-
948 152, 2008.

949 Prospero, J. M., Ginoux, P., Torres, O., Nicholson, S. E., and Gill, T. E.: Environmental characterization of global
950 sources of atmospheric soil dust identified with the Nimbus 7 Total Ozone Mapping Spectrometer (TOMS)
951 absorbing aerosol product, *Rev. Geophys.*, 40, 1002, DOI: 1010.1029/2000RG000095, 2002.

952 Rard, J. A., Habenschuss, A., and Spedding, F. H.: A review of the osmotic coefficients of aqueous calcium chloride
953 at 25 °C, *J. Chem. Eng. Data*, 22, 180-186, 1977.

954 Rard, J. A., and Miller, D. G.: Isopiestic determination of the osmotic and activity coefficients of aqueous
955 magnesium chloride solutions at 25 °C, *J. Chem. Eng. Data*, 26, 38-43, 1981.

956 Rard, J. A., Wijesinghe, A. M., and Wolery, T. J.: Review of the thermodynamic properties of Mg(NO₃)₂(aq) and
957 their representation with the standard and extended ion-interaction (Pitzer) models at 298.15 K, *J. Chem. Eng. Data*,
958 49, 1127-1140, 2004.

959 Ridley, D. A., Heald, C. L., Kok, J. F., and Zhao, C.: An observationally constrained estimate of global dust aerosol
960 optical depth, *Atmos. Chem. Phys.*, 16, 15097-15117, 2016.

961 Robinson, R. A., and Stokes, R. H.: *Electrolyte Solutions (Second Revised Edition)*, Butterworths, London, UK,
962 1959.

963 Romanias, M. N., El Zein, A., and Bedjanian, Y.: Heterogeneous Interaction of H₂O₂ with TiO₂ Surface under Dark
964 and UV Light Irradiation Conditions, *J. Phys. Chem. A*, 116, 8191-8200, 2012.

965 Romanias, M. N., Zeineddine, M. N., Gaudion, V., Lun, X., Thevenet, F., and Riffault, V.: Heterogeneous
966 Interaction of Isopropanol with Natural Gobi Dust, *Environ. Sci. Technol.*, 50, 11714-11722, 2016.

967 Santschi, C., and Rossi, M. J.: Uptake of CO₂, SO₂, HNO₃ and HCl on calcite (CaCO₃) at 300 K: Mechanism and
968 the role of adsorbed water, *J. Phys. Chem. A*, 110, 6789-6802, 2006.

969 Scanza, R. A., Mahowald, N., Ghan, S., Zender, C. S., Kok, J. F., Liu, X., Zhang, Y., and Albani, S.: Modeling Dust
970 as Component Minerals in the Community Atmosphere Model: Development of Framework and Impact on
971 Radiative Forcing, *Atmos. Chem. Phys.*, 15, 537-561, 2015.

972 Seinfeld, J. H., and Pandis, S. N.: *Atmospheric Chemistry and Physics: From Air Pollution to Climate Change*
973 (Third edition), Wiley Interscience, New York, 2016.

974 Shi, Z., Zhang, D., Hayashi, M., Ogata, H., Ji, H., and Fujie, W.: Influences of sulfate and nitrate on the
975 hygroscopic behaviour of coarse dust particles, *Atmos. Environ.*, 42, 822-827, 2008.

976 Sullivan, R. C., Moore, M. J. K., Petters, M. D., Kreidenweis, S. M., Roberts, G. C., and Prather, K. A.: Effect of
977 Chemical Mixing State on the Hygroscopicity and Cloud Nucleation Properties of Calcium Mineral Dust Particles,
978 *Atmos. Chem. Phys.*, 9, 3303-3316, 2009.

979 Tan, F., Tong, S. R., Jing, B., Hou, S., Liu, Q., Li, K., Zhang, Y., and Ge, M. F.: Heterogeneous reactions of NO₂
980 with CaCO₃-(NH₄)₂SO₄ mixtures at different relative humidities, *Atmos. Chem. Phys.*, 16, 8081-8093, 2016.

981 Tang, I. N., and Fung, K. H.: Hydration and Raman scattering studies of levitated microparticles: Ba(NO₃)₂,
982 Sr(NO₃)₂, and Ca(NO₃)₂, *J. Chem. Phys.*, 106, 1653-1660, 1997.

983 Tang, M. J., Thieser, J., Schuster, G., and Crowley, J. N.: Kinetics and Mechanism of the Heterogeneous Reaction of
984 N₂O₅ with Mineral Dust Particles, *Phys. Chem. Chem. Phys.*, 14, 8551-8561, 2012.

985 Tang, M. J., Whitehead, J., Davidson, N. M., Pope, F. D., Alfarra, M. R., McFiggans, G., and Kalberer, M.: Cloud
986 Condensation Nucleation Activities of Calcium Carbonate and its Atmospheric Ageing Products, *Phys. Chem.*
987 *Chem. Phys.*, 17, 32194-32203, 2015.

988 Tang, M. J., Cziczo, D. J., and Grassian, V. H.: Interactions of Water with Mineral Dust Aerosol: Water Adsorption,
989 Hygroscopicity, Cloud Condensation and Ice Nucleation, *Chem. Rev.*, 116, 4205-4259, 2016a.

990 Tang, M. J., Larish, W., Fang, Y., Gankanda, A., and Grassian, V. H.: Heterogeneous Reactions of Acetic Acid with
991 Oxide Surfaces: Effects of Mineralogy and Relative Humidity, *J. Phys. Chem. A*, 120, 5609-5616, 2016b.

992 Tang, M. J., Huang, X., Lu, K. D., Ge, M. F., Li, Y. J., Cheng, P., Zhu, T., Ding, A. J., Zhang, Y. H., Gligorovski,
993 S., Song, W., Ding, X., Bi, X. H., and Wang, X. M.: Heterogeneous reactions of mineral dust aerosol: implications
994 for tropospheric oxidation capacity, *Atmos. Chem. Phys.*, 17, 11727-11777, 2017.

995 Textor, C., Schulz, M., Guibert, S., Kinne, S., Balkanski, Y., Bauer, S., Bernsten, T., Berglen, T., Boucher, O., Chin,
996 M., Dentener, F., Diehl, T., Easter, R., Feichter, H., Fillmore, D., Ghan, S., Ginoux, P., Gong, S., Grini, A.,
997 Hendricks, J., Horowitz, L., Huang, P., Isaksen, I., Iversen, I., Kloster, S., Koch, D., Kirkevåg, A., Kristjansson, J.
998 E., Krol, M., Lauer, A., Lamarque, J. F., Liu, X., Montanaro, V., Myhre, G., Penner, J., Pitari, G., Reddy, S., Seland,
999 Ø., Stier, P., Takemura, T., and Tie, X.: Analysis and Quantification of the Diversities of Aerosol Life Cycles within
1000 AeroCom, *Atmos. Chem. Phys.*, 6, 1777-1813, 2006.

1001 Tobo, Y., Zhang, D. Z., Nakata, N., Yamada, M., Ogata, H., Hara, K., and Iwasaka, Y.: Hygroscopic mineral dust
1002 particles as influenced by chlorine chemistry in the marine atmosphere, *Geophys. Res. Lett.*, 36, L05817, doi:
1003 05810.01029/02008gl036883, 2009.

1004 Tobo, Y., Zhang, D., Matsuki, A., and Iwasaka, Y.: Asian Dust Particles Converted into Aqueous Droplets under
1005 Remote Marine Atmospheric Conditions, *Proc. Natl. Acad. Sci. U. S. A.*, 107, 17905-17910, 2010.

1006 Tong, S. R., Wu, L. Y., Ge, M. F., Wang, W. G., and Pu, Z. F.: Heterogeneous Chemistry of Monocarboxylic Acids
1007 on α-Al₂O₃ at Different Relative Humidities, *Atmos. Chem. Phys.*, 10, 7561-7574, 2010.

1008 Uno, I., Eguchi, K., Yumimoto, K., Takemura, T., Shimizu, A., Uematsu, M., Liu, Z., Wang, Z., Hara, Y., and
1009 Sugimoto, N.: Asian Dust Transported One Full Circuit around the Globe, *Nature Geosci.*, 2, 557-560, 2009.
1010 Usher, C. R., Michel, A. E., and Grassian, V. H.: Reactions on Mineral Dust, *Chem. Rev.*, 103, 4883-4939, 2003.
1011 Vlasenko, A., Sjogren, S., Weingartner, E., Gaggeler, H. W., and Ammann, M.: Generation of submicron Arizona
1012 test dust aerosol: Chemical and hygroscopic properties, *Aerosol Sci. Technol.*, 39, 452-460, 2005.
1013 Vlasenko, A., Sjogren, S., Weingartner, E., Stemmler, K., Gaggeler, H. W., and Ammann, M.: Effect of Humidity
1014 on Nitric Acid Uptake to Mineral Dust Aerosol Particles, *Atmos. Chem. Phys.*, 6, 2147-2160, 2006.
1015 Vlasenko, S. S., Su, H., Pöschl, U., Andreae, M. O., and Mikhailov, E. F.: Tandem configuration of differential
1016 mobility and centrifugal particle mass analysers for investigating aerosol hygroscopic properties, *Atmos. Meas.*
1017 *Tech.*, 10, 1269-1280, 2017.
1018 Wang, L. Y., Zhang, Y. H., and Zhao, L. J.: Raman spectroscopic studies on single supersaturated droplets of
1019 sodium and magnesium acetate, *J. Phys. Chem. A*, 109, 609-614, 2005.
1020 Wex, H., Petters, M. D., Carrico, C. M., Hallbauer, E., Massling, A., McMeeking, G. R., Poulain, L., Wu, Z.,
1021 Kreidenweis, S. M., and Stratmann, F.: Towards closing the gap between hygroscopic growth and activation for
1022 secondary organic aerosol: Part 1 – Evidence from measurements, *Atmos. Chem. Phys.*, 9, 3987-3997, 2009.
1023 Wexler, A. S., and Seinfeld, J. H.: 2nd generation inorganic aerosol model, *Atmos. Environ.*, 25, 2731-2748, 1991.
1024 Zhang, Y., Mahowald, N., Scanza, R. A., Journet, E., Desboeufs, K., Albani, S., Kok, J. F., Zhuang, G., Chen, Y.,
1025 Cohen, D. D., Paytan, A., Patey, M. D., Achterberg, E. P., Engelbrecht, J. P., and Fomba, K. W.: Modeling the
1026 global emission, transport and deposition of trace elements associated with mineral dust, *Biogeosciences*, 12, 5771-
1027 5792, 2015.
1028 Zhang, Y. H., Choi, M. Y., and Chan, C. K.: Relating hygroscopic properties of magnesium nitrate to the formation
1029 of contact ion pairs, *J. Phys. Chem. A*, 108, 1712-1718, 2004.
1030 Zieger, P., Vaisanen, O., Corbin, J. C., Partridge, D. G., Bastelberger, S., Mousavi-Fard, M., Rosati, B., Gysel, M.,
1031 Krieger, U. K., Leck, C., Nenes, A., Riipinen, I., Virtanen, A., and Salter, M. E.: Revising the hygroscopicity of
1032 inorganic sea salt particles, *Nature Communications*, 8, 15883, doi: 15810.11038/ncomms15883, 2017.
1033